Effects of a Fluorinated Donor Polymer on the Morphology, Photophysics, and Performance of All-Polymer Solar Cells based on Naphthalene Diimide-Arylene Copolymer Acceptors

Duyen K. Tran,[†] Nagesh B. Kolhe, [†] Ye-jin Hwang,[||] Daiki Kuzuhara,[‡] Tomoyuki Koganezawa,[§] and Samson A. Jenekhe[,†]*

[†]Department of Chemical Engineering and Department of Chemistry, University of Washington, Seattle, Washington 98195-1750, United States

[||]Department of Chemistry and Chemical Engineering, Inha University, 100 Inha-ro, Michuhol-gu, Incheon, Republic of Korea

[‡]Faculty of Science and Engineering, Iwate University, 4-3-5 Ueda, Morioka, Iwata, 020-8551, Japan

[§]Industry Application Division, Japan Synchrotron Radiation Research Institute, Sayo, Hyogo, 679-5198, Japan

KEYWORDS: All-polymer solar cells, Fluorinated donor polymer, Naphthalene Diimide-Arylene Copolymer, Vertical phase stratification, Thick-film active layer, Blend Morphology.

ABSTRACT: Naphthalene diimide (NDI)-biselenophene copolymer (PNDIBS) and NDI-selenophene copolymer (PNDIS) and the fluorinated donor polymer PM6 were used to investigate how a fluorinated polymer component affects the morphology and performance of all-polymer solar cells (all-PSCs). Although the PM6:PNDIBS blend system exhibits a high open-circuit voltage (V_{oc} = 0.925 V) and desired low optical bandgap energy loss (E_{loss} = 0.475 eV), the overall power conversion efficiency (PCE) was 3.1%. In contrast, PM6:PNDIS blends combine a high V_{oc} (0.967 V) with a high fill factor (FF = 0.70) to produce efficient all-PSCs with 9.1% PCE. Furthermore, the high performance PM6:PNDIS all-PSCs could be fabricated by various solution processing approaches and at active layer thickness as high as 300 nm without compromising photovoltaic efficiency. The divergent photovoltaic properties of PNDIS and PNDIBS when paired respectively with PM6 are shown to originate from the starkly different blend morphology and blend photophysics. Efficient PM6:PNDIS blend films were found to exhibit a vertical phase stratification along with lateral phase separation while the molecular packing had a predominant *face-on* orientation. Bulk lateral phase separation with both *face-on* and *edge-on* molecular orientations featured in the poor performing PM6:PNDIBS blend films. Enhanced charge photogeneration and suppressed geminate and bimolecular recombinations with 99% charge collection probability found in PM6:PNDIS blends strongly differ from the poor charge collection probability (66%) and high electron-hole pair recombination seen in PM6:PNDIBS. Our findings demonstrate that beyond the generally expected enhancement of V_{oc}, a fluorinated polymer component in all-PSCs can also exert a positive or negative influence on photovoltaic performance via the blend morphology and blend photophysics.

INTRODUCTION

All-polymer solar cells (all-PSCs), in which the active layer is comprised of a binary blend of an electron-donating (donor) polymer and an electron-accepting (acceptor) polymer, have garnered significant research efforts over the past several years, leading to great strides in terms of device performance.[1-4] Although the power conversion efficiency (PCE) of all-PSCs lags the efficiency of small molecule non-fullerene acceptors (SM-NFAs) based solar cells,[5, 6] all-PSCs have unique advantages over SM-NFA devices, including superior photo- and electro-chemical stability,[7, 8] enhanced thermal and mechanical robustness,[9-11] and enhanced rheological properties which are ideal for large scale film coating.[10, 11] These advantages make all-PSCs promising candidates for large-scale manufacturing.[8, 11-13] The key parameters limiting the device efficiency of all-PSCs have long been identified as the generally low fill factor (FF)[1-4, 14] and the modest open-circuit voltage (V_{oc}).[1-3, 15] The low V_{oc} (< 1V) is mainly due to the large optical bandgap energy loss ($E_{loss} = E_g - eV_{oc} > 0.6$ eV),[1-3, 12] while the poor FF originates primarily from non-optimal blend morphology and inefficient charge extraction at the organic/metal interfaces.[1-3] Several strategies have been explored for tailoring the blend morphology of all-PSCs, including thermal annealing,[16-18] solvent vapor annealing,[14] room-temperature aging,[8, 19] co-solvents,[20] solvent processing additives,[12, 17, 21, 22] side chain engineering,[23-25] and random copolymerization,[26-29] whereby some systems could achieve near unity internal quantum efficiency (IQE).[14, 27, 28]

A potential strategy to improve the V_{oc} of all-PSCs is incorporation of fluorine atoms into the molecular structure of either the donor or the acceptor polymer. Fluorination has been demonstrated to be an effective molecular design strategy to enhance the photovoltaic properties, especially in SM-NFA solar cells.[5, 6, 30, 31] Effects of fluorination include lowering the highest occupied molecular orbital (HOMO) and the lowest unoccupied molecular orbital (LUMO) energy

levels,[32] enhancing the crystallinity of the blend components and forming a favorable blend morphology due to F-F intermolecular interactions,[29, 33-35] altering the dielectric constant of the materials,[29, 30, 36, 37] suppressing charge recombination and enhancing charge photogeneration,[35, 38] and increasing charge carrier mobility.[39] Despite the impressive performance of SM-NFA solar cells based on fluorinated donor polymers, application of such fluorinated donor polymers in all-PSCs is surprisingly rare; in the few known examples, the fluorinated donor polymers, poly[(2,6-(4,8-bis(5-(2-ethylhexyl-3-fluoro)thiophen-2-yl)-benzo[1,2-b:4,5-b']dithiophene))-alt-(5,5-(1',3'-di-2-thienyl-5',7'-bis(2-ethylhexyl)benzo[1',2'-c:4',5'-c']dithiophene-4,8-dione)], (PBDB-TF or PM6) shown in Figure 1a has been paired with various acceptor polymers having a ladder-type fused ring co-monomer in their repeating units.[21, 40, 41] The pairing of PM6 with such fused-ring acceptor polymers such as PZ1,[40] PFBDT-IDTIC,[21] and PN1[41] has resulted in high performance all-PSCs with PCEs of 10 – 11% and V_{oc} of 0.96 – 1.0V.[21, 40, 41] Surprisingly, effects of a fluorinated donor polymer on the performance of all-PSCs based on naphthalene diimide (NDI) copolymer acceptors have yet to be explored. NDI-arylene copolymer acceptors have been widely studied as materials for constructing highly efficient all-PSCs.[8, 12, 42-44] Indeed, our group[8, 12, 28] and others[13, 45-47] have showed that all-PSCs with PCEs as high as 8-10% can be achieved by pairing various NDI-arylene copolymers with the non-fluorinated derivative of PM6, i.e. PBDB-T. However, because numerous factors determine the compatibility, nanoscale morphology, and PCE of all-PSC devices, *a priori* prediction of how the fluorination of the donor polymer could influence the performance of all-PSCs based on NDI-arylene copolymer acceptors is not possible.

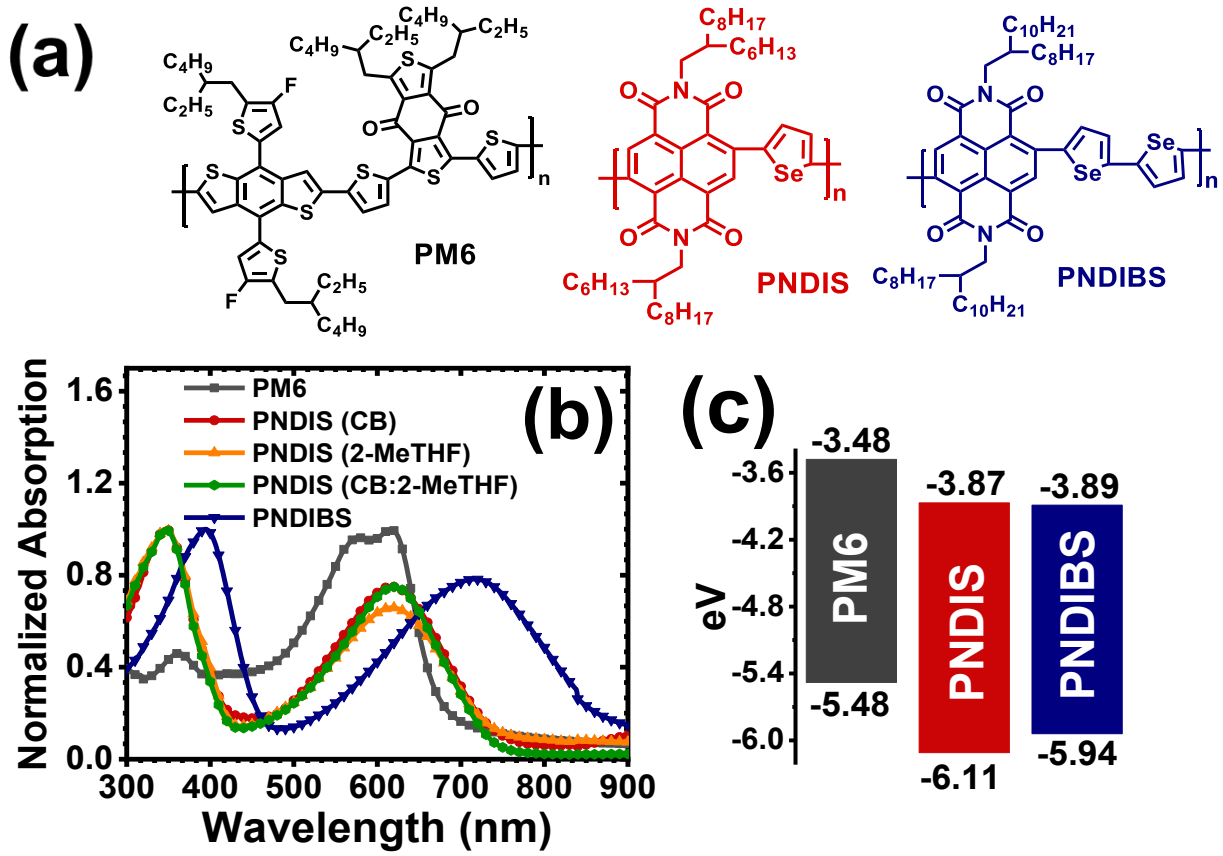

Figure 1. (a) Molecular structures of donor polymer, PM6, and acceptor polymers, PNDIS and PNDIBS. (b) Normalized thin-film optical absorption spectra of the donor and acceptor polymers processed from different solvents. (c) HOMO/LUMO energy levels of the donor and acceptor polymers.

In this paper, we report an investigation of the effects of fluorination of the donor polymer on the blend morphology, blend photophysics, and photovoltaic properties of all-PSCs based on NDI-arylene copolymer acceptors. We found that pairing the fluorinated donor polymer PM6 with two different related NDI-arylene copolymers – NDI-biselenophene copolymer (PNDIBS) and NDI-selenophene copolymer (PNDIS) shown in Figure 1a – resulted in dramatically different outcomes and very divergent observations. Contrary to expectations from the known high performance (> 9% PCE) of PBDB-T:PNDIBS all-PSCs,[12] blends of the fluorinated donor polymer PM6 with PNDIBS gave rise to substantially inferior photovoltaic properties with a maximum PCE of 3.1%. In contrast, blends of PM6 with PNDIS could be used to develop all-PSCs with a maximum PCE of over 9%. Furthermore, these efficient PM6:PNDIS blend all-PSCs were found to be relatively insensitive to device processing methods and to active layer thickness of up to 300 nm. Detailed comparative studies of the PM6:PNDIBS and PM6:PNDIS blend systems show that the divergent effects of the fluorinated donor polymer on the photovoltaic properties originate from the stark differences in blend morphology and blend photophysics. We show that the PM6:PNDIBS blend system exhibits a lateral bulk phase separation in which both *face-on* and *edge-on* molecular orientations are displayed. In contrast, the bulk thin films of the PM6:PNDIS blend system are characterized by prominent vertical phase stratification and some lateral phase segregation in conjunction with predominant *face-on* molecular orientation. The photophysics of PM6:PNDIBS blends was characterized by low charge photogeneration rate, high electron-hole pair recombination rate, and poor charge collection probability (P(E,T) = 65.5%). In stark difference, the PM6:PNDIS blend photophysics featured enhanced charge photogeneration rate, suppressed geminate and bimolecular recombinations and near unity charge collection probability (P(E,T) = 99.1%). These results show that in addition to the generally expected enhancement of V_{oc},

fluorination of a polymer component of all-PSCs can also dramatically influence the blend morphology and blend photophysics with consequent net negative or positive impact on the photovoltaic efficiency.

EXPERIMENTAL METHODS

Materials. The donor polymer, PM6, was purchased from Solarmer Energy Inc (M_n = 14.6 kDa, M_w = 38 kDa, $Đ$ = 2.60) (Irwindale, CA, United States) while PNDIS and PNDIBS were previously synthesized in our lab.[8, 12] Optical absorption spectra were obtained from a PerkinElmer Lambda 900 UV-vis/near-IR spectrophotometer. Polymer molecular weight information was obtained with gel-permeation chromatography (GPC) eluting with chloroform at room temperature (25ºC) for PNDIS (M_n = 22.1 kDa, M_w = 64.9 kDa, $Đ$ = 2.94) whereas the GPC characterization was done in chlorobenzene at room temperature for PNDIBS (M_n = 114.6 kDa, M_w = 218 kDa, $Đ$ = 1.90).

Cyclic Voltammetry. Cyclic voltammetry (CV) experiments were done on an EG&G Princeton Applied Research Potentiostat/Galvanostat (model 273A). A three-electrode cell was used, using platinum wire electrodes as both counter and working electrode. Ag/Ag^+ (Ag in 0.01 M $AgNO_3$ solution) was used as a reference electrode. The films of the polymer were coated onto the Pt wires by dipping the wires into polymer solutions of the polymers (PM6, PNDIS, and PNDIBS) and drying the coated films at 25 °C. All the CV measurements were carried out in 0.1 M tetrabutylammonium hexafluorophosphate (Bu_4NPF_6) electrolyte solution in acetonitrile at a scan rate of 50 mV/s. The reduction and oxidation potentials were referenced to the Fc/Fc^+ couple by using ferrocene as an internal standard. The LUMO and HOMO energy levels were estimated using a ferrocene value of −4.8 eV with respect to vacuum level. The LUMO and HOMO energy levels were determined using the equations $E_{LUMO} = -(eE_{red\text{-}onset} + 4.8)$ and $E_{HOMO} = -(eE_{ox\text{-}onset} + 4.8)$, respectively.

Fabrication and Characterization of all-PSCs. Solar cells devices were fabricated with an inverted architecture of ITO/ZnO/PEI/Blend/MoO_3/Ag. ITO-coated substrates (15 Ω/square, Shanghai B. Tree Tech, Shanghai, China) were cleaned sequentially in ultrasonic baths with acetone, deionized water, and isopropyl alcohol for 30 min, dried using nitrogen gas, and followed by 10 mins of O_2 plasma cleaning. The ZnO precursor solution was spin-coated onto the ITO and followed by thermal annealing at 250 °C for 30 min to make ~30 nm thick ZnO layer. A 0.05 wt% solution of polyethylenimine (PEI) in 2-methoxyethanol was spin-coated onto the ZnO layer and dried at 120 °C for 10 min. The PM6:PNDIS (1:0.6 wt/wt) blends were prepared in chlorobenzene (CB), mixed and stirred overnight at 85ºC in the glovebox. A mixture of 0.25% (v/v) of 1,8-diiodooctane (DIO) and 0.25% (v/v) of 1,8-octanedithiol (ODT) was added into the PM6:PNDIS blend solutions. Similarly, the PM6:PNDIBS (1:0.4 wt/wt) blends were prepared in chlorobenzene, mixed and stirred overnight at 85ºC in the glovebox. 0.5% (v/v) diphenyl ether (DPE) was added to the blend solution as a processing additive. For the sake of comparisons, the PBDB-T:PNDIS and PBDB-T:PNDIBS blends were prepared in the exact same conditions as the optimized PM6:PNDIS and PM6:PNDIBS blends, respectively. In case of device fabrication using co-solvents, the PM6:PNDIS (1:0.6 wt/wt) blends were prepared in a mixture of CB and 2-methyltetrahydrofuran (2-MeTHF) (CB:2-MeTHF) at the optimal ratio of 70:30 (v:v), mixed and stirred overnight at 65ºC in the glovebox. No processing additive was used when devices were processed from CB:2-MeTHF co-solvents. The blend solutions were spin-coated at 1000 rpm for 50s, followed by thermal annealing at 110ºC for 10 min in the Argon-filled glovebox. All the active layers had a thickness of 102 ± 3 nm. MoO_3 (0.5 nm) and Ag (100 nm) were thermally deposited onto the active layer. An aperture mask with area of 3.14 mm^2 was applied during measurements to define the illuminated device area. After evaporation of the electrode, the

photovoltaic cells were tested under AM 1.5G solar illumination at 100 mW/cm^2 in ambient air by using a solar simulator (Model 16S, Solar Light Co., Philadelphia, PA) with a 200W Xenon Lamp Power Supply (Model XPS 200, Solar Light Co., Philadelphia, PA) calibrated by NREL certified Si photodiode (Model 1787-04, Hamamatsu Photonics K.K., Japan) and a HP4155A semiconductor parameter analyzer (Yokogawa Hewlett Packard, Japan). After the *J-V* measurements, the external quantum efficiency (EQE) spectra were measured by using a solar cell quantum efficiency measurement system (Model QEX10, PV Measurements, Inc., Boulder, CO) with a 2 mm^2 (2 mm × 1 mm) size masked incident light source and TF Mini Super measurement apparatus for multiple devices in a single substrate. The EQE system was calibrated with a Si photodiode before measurement.

Fabrication and Characterization of SCLC Devices. Current-voltage (*J-V*) characteristics of the space-charge limited current (SCLC) devices were measured by using a HP4155A semiconductor parameter analyzer (Yokogawa Hewlett-Packard, Tokyo). The carrier mobility was deduced by fitting the *J-V* curves to the Mott−Gurney equation,

$$J = \frac{9}{8}\varepsilon_0\varepsilon\mu\frac{V^2}{L^3}$$

where J is the current density, ε_0 is the permittivity of free space, ε is the relative permittivity, μ is the zero-field mobility, V is the applied voltage, L is the thickness of active layer.

The SCLC device structures for electron-only and hole-only were ITO/ZnO/PEI/Blend/LiF (1nm)/Al (100nm) and ITO/PEDOT: PSS/Blend/MoO_3 (7.5nm)/Ag (100nm), respectively. Each active layer of both neat and blend films was processed at the optimized all-PSC device conditions as described above and spin-coated at 1000 rpm for 50s and followed by thermal annealing at 110^{o}C for 10 min inside glovebox.

AFM Imaging. Atomic force microscopy (AFM) characterization of the surface morphology was done on the active layers of the actual polymer solar cells, used in the photovoltaic measurements, by using a Bruker Dimension scanning probe microscope (SPM) system.

2D-GIWAXS. Grazing incidence X-ray scattering (GIWAXS) experiments were conducted at the Japan Synchrotron Radiation Facility SPring-8 by using the beamlines BL46XU. Thin film samples of the neat donor polymer (PM6) and acceptor polymers (PNDIS and PNDIBS) were spin-coated on the top of glass substrates and annealed at 110 °C for 10 min. The binary blend films were prepared in the same manner as the actual all-PSC devices on ZnO/PEI-coated ITO substrates. The X-ray beam was monochromatized by a double-crystal Si(111) monochromator, and the X-ray energy in this experiment was 12.40 keV (λ = 0.1 nm). The angle of incident X-ray to sample surface was 0.12° with a Huber diffractometer. The scattered profile from the film sample was detected using an area detector (PILATUS 300K) for 1 s at room temperature, and the distance between the sample and detector was 175.0 mm. The crystal coherence length (L_c) of samples was determined by using the Scherrer equation: $L_c = 2\pi K/\Delta q$, where K is a shape factor (typically 0.89) and Δq is the full width at half-maximum (FWHM) of the diffraction peak. Here, the L_c (100) was obtained from the FWHM of the (100) diffraction peak in the-plane (q_{xy}) line cut.

RESULTS AND DISCUSSION

Optical Properties and Electronic Structure. The thin film absorption spectra of the donor polymer PM6 and the acceptor polymers PNDIS and PNDIBS are presented in Figure 1b. Two characteristics peaks at around 362 nm and 570 – 620 nm representing π-π^* transition and intramolecular charge transfer (ICT) band, respectively, were observed in PM6 in agreement with prior reports.[40, 48] PNDIS exhibits two peaks at about 348 and 618 nm and an absorption onset (λ_{onset}) at around 740 nm corresponding to an optical bandgap (E_g^{opt}) of 1.67 eV. PNDIBS has a

clearly red-shifted absorption with π-π* and ICT peaks at 394 and 716 nm, respectively, and an λ_{onset} at 885 nm (E_g^{opt} = 1.40 eV). The red-shifted absorption of PNDIBS compared to PNDIS is due to the longer conjugation length as well as the effect of the stronger electron-donating nature of the biselenophene moiety on the ICT absorption band compared to the selenophene moiety in PNDIS. These thin film absorption spectra are in accord with previous reports.[8, 12, 20, 49]

The thin film and solution absorption spectra in neat 2-MeTHF and CB:2-MeTHF co-solvents are shown in Figures 1b and S1b, respectively, since the CB:2-MeTHF co-solvents will also be used to fabricate all-PSC devices. We note that only the absorption profiles of PNDIS in the various co-solvents were collected and presented due to the limited solubility of PM6 and PNDIBS in 2-MeTHF. Although the thin film absorption spectra of PNDIS deposited from CB, 2-MeTHF, and CB:2-MeTHF were virtually similar (Figure 1b), their corresponding solution absorption spectra (Figure S1b) showed distinct bathochromic shifts. The ICT band and the λ_{onset} of PNDIS in 2-MeTHF as well as in CB:2-MeTHF were red-shifted by about 42 nm relative to those in CB. Given that the dielectric constant (ε) of 2-MeTHF (ε = 6.97) is larger than of CB (ε = 5.62), the observed bathochromic shift of the absorption of PNDIS with increasing solvent polarity reflects the greater charge separation and ICT character in the electronic ground state.[50, 51] Alternatively, the solution absorption spectra indicate that 2-MeTHF is a theta solvent for PNDIS, which means PNDIS chains would prefer to stay in 2-MeTHF phase and are likely to undergo conformational changes to become less coiled,[52, 53] and thereby increase the effective conjugated length. In this case, using a mixture of chlorobenzene and 2-methyltetrahydrofuran as co-solvents for device processing could enable independent tuning of the aggregation rates of PM6 and PNDIS. In particular, the PNDIS chains in the low boiling point solvent, 2-MeTHF (T_b = 80.2°C), undergo a quick film-forming kinetics to form relatively pure domains with smaller domain sizes due to the

fast evaporation rate of 2-MeTHF whereas the PM6 chains in the higher boiling point solvent, CB (T_b = 132ºC), slowly aggregate to form its own domains. As a result, the aggregation rates of PM6 and PNDIS can be independently tailored via their differential solubility in the CB:2-MeTHF co-solvent and the differential boiling point of the solvents. Use of such a co-solvent system thus eliminates the need for processing additives in solution-based active layer fabrication.

The LUMO and HOMO energy levels of the component polymers shown in Figure 1c were measured using cyclic voltammetry, and the resulting oxidation and reduction cyclic voltammograms are shown in Figure S2. The LUMO and HOMO energy levels of the donor polymer PM6 are found to be -3.48 eV and -5.48 eV, respectively, which are consistent with previous report.[48] The LUMO energy levels of the acceptor polymers, PNDIS and PNDIBS, are essentially identical at -3.87 eV and -3.89 eV, respectively. The HOMO energy level of PNDIBS (HOMO = -5.94 eV) is higher lying than that of PNDIS (HOMO = -6.11 eV) mainly due to the stronger electron-donating nature of the biselenophene unit relative to the selenophene unit, which are also in good agreement with previous reports.[8, 12] As Figure 1c suggests, the driving forces for exciton dissociation (ΔHOMO and ΔLUMO) are comparable between PM6:PNDIS blends and PM6:PNDIBS blends.

Photovoltaic Properties. The photovoltaic properties of the binary PM6:PNDIS and PM6:PNDIBS blends were investigated by fabricating and characterizing all-PSCs with an inverted device architecture: ITO/ZnO/PEI/Blend/MoO_3/Ag, where polyethyleneimine (PEI) is used as the cathode buffer layer.[54] Thin film absorption spectra and the energy levels of the blend components (PM6, PNDIS, and PNDIBS) are shown in Figures 1b and 1c, respectively. The PM6:PNDIS and PM6:PNDIBS all-PSC devices were fully optimized by varying the donor : acceptor (D:A) ratio, choice of solvent additives, and thermal annealing at different temperatures

(Tables S2 and S3). The optimal processing conditions for the PM6:PNDIS blends included spin-coating the chlorobenzene blend solution of 1:0.6 (wt:wt) D:A ratio with a mixture of solvent processing additives (0.25% (v/v) 1,8-octanedithiol (ODT) and 0.25% (v/v) 1,8-diiodooctane (DIO)) followed by thermal annealing at 110°C for 10 min in an Argon-filled glovebox. The PM6:PNDIBS blends were optimized separately by spin-coating the chlorobenzene blend solution of 1:0.4 (wt:wt) D:A ratio with 0.5% (v/v) diphenyl ether (DPE) solvent processing additive followed by thermal annealing at 110°C for 10 min in the glovebox. The *J-V* curves and the EQE spectra of optimized PM6:PNDIS, PM6:PNDIBS all-PSC devices are presented in Figure 2, and the corresponding photovoltaic parameters are summarized in Table 1. The PBDB-T:PNDIS devices and PBDB-T:PNDIBS devices were fabricated at the exact same optimal processing conditions for the PM6:PNDIS devices and PM6:PNDIBS devices, respectively. The *J-V* curves and the EQE spectra of PBDB-T:PNDIS and PBDB-T:PNDIBS all-PSC devices are shown in Figure S3, and the photovoltaic parameters are summarized in Table S1.

All-PSC devices fabricated from the PM6:PNDIS binary blend at 1:0.6 (wt:wt) D:A ratio had an average PCE of 7.55% with a J_{sc} of 11.89 mA/cm^2, a V_{oc} of 0.962 V, and a FF of 0.66 (Table S2). Through screening of processing additives, we found that addition of both 0.25% (v/v) of DIO and 0.25% (v/v) of ODT to the chlorobenzene solvent resulted in significant enhancement in the photovoltaic parameters (J_{sc}, FF, and PCE) (Table S2). The combination of 0.25% ODT and 0.25% DIO as solvent additives was found to be more effective than using a single solvent additive mainly due to the suppressed aggregation and the optimal domain sizes as evidenced by the smoother surface of the blend films from AFM images (Figure S4a) and the increased spatial frequency from the power spectral density (Figure S4b). Although the V_{oc} was unaffected by the solvent additives (V_{oc} = 0.97 V), the J_{sc} improved from 11.89 mA/cm^2 to 13.45 mA/cm^2 while the

FF increased from 0.66 to 0.70. As a result, the optimized PM6:PNDIS all-PSC devices exhibited a maximum PCE of 9.07% (Table 1). This efficiency (9.1%) seen in PM6:PNDIS blends is the highest observed so far for this acceptor polymer in all-PSC devices.[8, 20, 49]

Table 1. Photovoltaic Properties of Optimized PM6:PNDIS and PM6:PNDIBS. All Active Layers were Thermally Annealed at 110°c for 10 min.

Blend	J_{sc} (mA/cm^2)	V_{oc} (V)	FF	PCE_{ave}[(a)] (%)	$J_{sc}^{calc.}$ (mA/cm^2)	R_{sh} (Ωcm^2)	R_s (Ωcm^2)
PM6:PNDIS	13.45 (13.14±0.13)	0.967 (0.960±0. 014)	0.70 (0.68±0. 02)	9.07 (8.63±0.36)	13.25	3546.1 (2351.8±1053.8)	6.96 (8.53±1.14)
PM6:PNDIBS	6.72 (6.32±0.18)	0.925 (0.927±0. 005)	0.50 (0.50±0. 01)	3.11 (2.93±0.08)	6.52	581.06 (551.8±55.95)	18.35 (22.29±2.82)

(a) Average of over 12 devices.

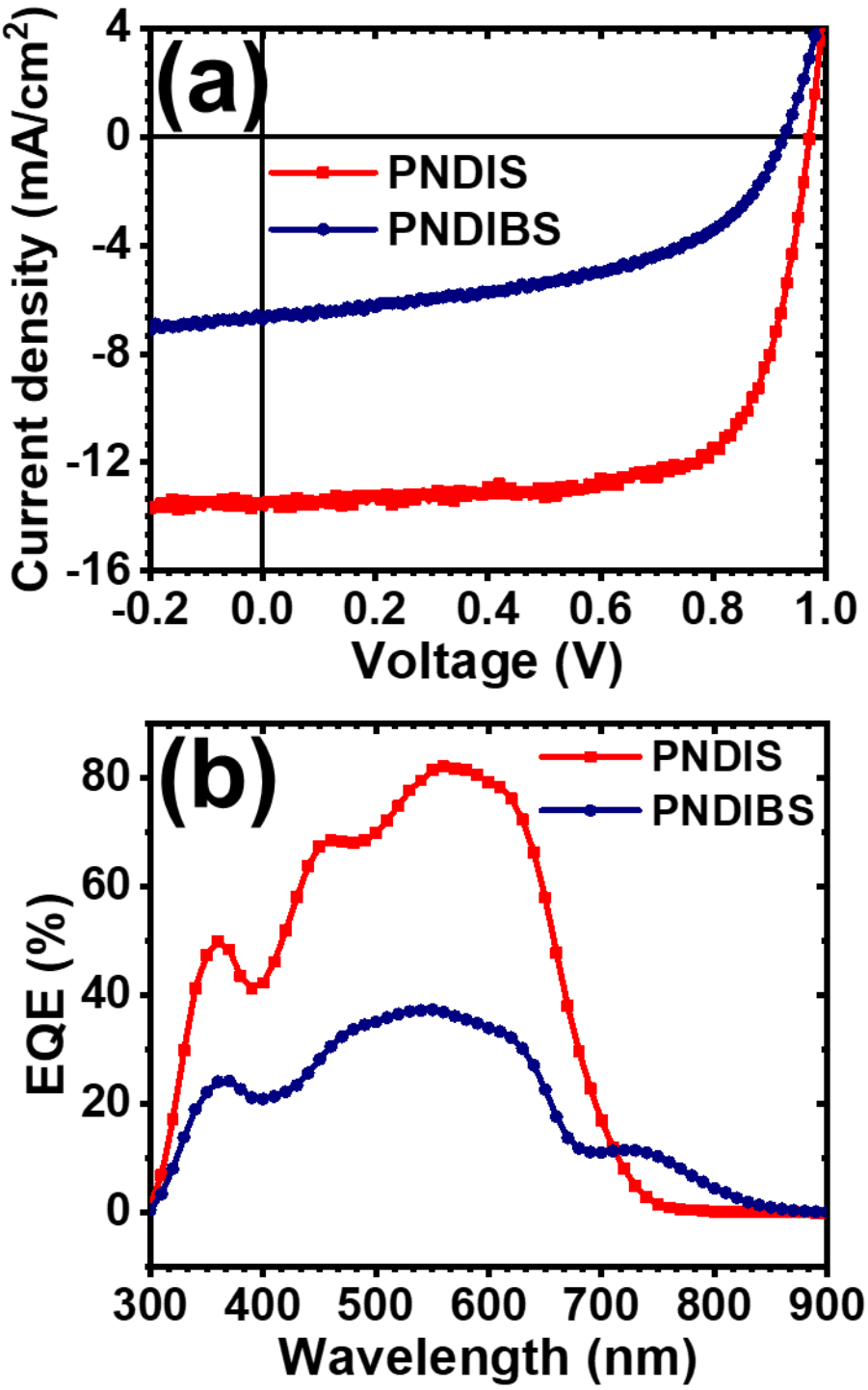

Figure 2. (a) *J-V* curves for the optimized PM6:PNDIS and PM6:PNDIBS devices processed from chlorobenzene. (b) EQE spectra for the optimized PM6:PNDIS and PM6:PNDIBS devices processed from chlorobenzene.

The similarly optimized PM6:PNDIBS blend devices have rather poor photovoltaic properties. The best performing PM6:PNDIBS blend devices had a PCE of 3.11% with a low J_{sc} of 6.72 mA/cm^2, a V_{oc} of 0.925V, and an FF of 0.50 (Table 1). While the marginal drop in V_{oc} is most likely due to the lower-lying LUMO energy level of PNDIBS compared to PNDIS (Figure 1c), the markedly inferior J_{sc} and FF can be attributed to the suboptimal morphology of the PM6:PNDIBS blends, which likely exaggerated charge recombination and inhibited efficient charge transport. Unlike the PM6:PNDIS blends, the use of solvent additives in the processing of PM6:PNDIBS blends led to only a marginal improvement in the photovoltaic properties (Table S3); for example, raising the PCE from 3.11% to 3.36-3.47% by using either 0.5% (v/v) DPE or DIO. This lack of effectiveness of processing additives suggests that the morphology of PM6:PNDIBS blends is trapped in a state inaccessible to fine-tuning by various optimization conditions.

The photovoltaic properties of the PM6:PNDIS and PM6:PNDIBS devices are staggeringly different from those of the all-PSC devices fabricated from the non-fluorinated donor polymer, PBDB-T. For the sake of comparison, the PBDB-T:PNDIS and PBDB-T:PNDIBS devices were fabricated at the exact optimized conditions of the PM6:PNDIS and PM6:PNDIBS devices, respectively. The photovoltaic parameters are summarized in Table S1 whereas the *J*-*V* curves and the EQE spectra are shown in Figure S3. The PBDB-T:PNDIS devices exhibited an average J_{sc} of 14.8 mA/cm^2, an average V_{oc} of 0.827 V, and an average FF of 0.61, leading to an average PCE of 7.5%. The PBDB-T:PNDIBS all-PSCs showed comparable device performance relative to the PBDB-T:PNDIS devices. In particular, the J_{sc} and V_{oc} were simultaneously enhanced (J_{sc} = 15.6 mA/cm^2, V_{oc} = 0.85 V) while the FF was slightly reduced to 0.58; thus, the best performing PBDB-T:PNDIBS had a PCE of 7.9%. We note that the photovoltaic parameters of PBDB-T:PNDIBS all-PSCs are slightly lower than our previous report[12] due to the differences in processing

conditions. Nevertheless, the observed substantial difference in the photovoltaic properties of the fluorinated donor polymer PM6 compared to PBDB-T in all-PSCs is fundamentally interesting. The remaining of the manuscript will address the underlying reasons that drive the deviations in the device performance of PM6:PNDIS and PM6:PNDIBS blends.

We also explored an alternative simpler optimization strategy to the device fabrication process by using a co-solvent system consisting of chlorobenzene and 2-methyltetrahydrofuran at various ratios (Table S4). In addition, we used the CB:2-MeTHF solvent system to examine the effects of the active layer thickness on the photovoltaic properties of the PM6:PNDIS all-PSC devices. In terms of the overall photovoltaic performance, the CB:2-MeTHF co-solvent processed optimized PM6:PNDIS devices (Table 2) are quite comparable to those processed with the aid of processing additives (Table 1). The *J-V* curves for PM6:PNDIS devices processed from CB:2-MeTHF co-solvents at various active layer thicknesses are presented in Figure 3a. All-PSC devices fabricated from the optimized CB:2-MeTHF co-solvents (Table S4) showed an average PCE of 8.41% with a high J_{sc} of 14.13 mA/cm^2, a V_{oc} of 0.963 V, and an FF of 0.62 (Table 2). The maximum PCE of 8.71% (J_{sc} = 14.72 mA/cm^2, V_{oc} = 0.96 V, and FF = 0.61) obtained for a 200-nm active layer is quite comparable to the 9.07% achieved with processing additives. These results were achieved by utilizing the difference in solubility of the donor and the acceptor polymer in 2-MeTHF to independently tune the aggregation rates of PM6 and PNDIS in the blend, enabling the self-organization of the polymer blends into optimal nanoscale morphology without using solvent additives. We conclude that that the PM6:PNDIS blend system is highly versatile, insensitive to processing methods, and is capable of yielding highly efficient all-PSC devices.

The dependencies of the photovoltaic parameters (J_{sc}, V_{oc}, FF, and PCE) on the active layer thicknesses are shown in Figures 3c – 3f. The V_{oc} is observed to be relatively constant at around

0.96 – 0.97V across all thicknesses whereas the FF progressively decreases from 0.63 to 0.58 as the thickness increased from 100 to 300 nm. The photocurrent density reaches a maximum value of 14.72 mA/cm^2 at 200 nm (Figure 3c). The maximum PCE peaks at 8.71% at 200 nm and decreases to 8.20% at 300 nm (Table 2 and Figure 3f). The minimal changes of the PCE of PM6:PNDIS all-PSC devices with the active layer thickness clearly indicate that this blend system is insensitive to both the processing methods and the film thicknesses, which are highly desirable for future commercial applications of all-PSCs.

Table 2. Photovoltaic Properties of Optimized PM6:PNDIS Devices Processed at the Optimized CB:2-MeTHF Co-solvents Without Using a Processing Solvent Additive at Various Active Layer Thicknesses. All Active Layers were Thermally Annealed at 110°C for 10 min.

Blend	J_{sc} (mA/cm^2)	V_{oc} (V)	FF	PCE$_{ave}$[(a)] (%)	$J_{sc}^{calc.}$ (mA/cm^2)	R_{sh} (Ωcm^2)	R_s (Ωcm^2)
100 nm	13.10 (13.04±0.13)	0.973 (0.964±0.005)	0.626 (0.629±0.004)	7.98 (7.90±0.08)	13.05	1052.3 (942.8±153.0)	7.39 (7.35±0.22)
200 nm	14.72 (14.13±0.77)	0.964 (0.963±0. 001)	0.614 (0.619±0.028)	8.71 (8.41±0.17)	14.08	997.0 (878.5±77.7)	8.97 (9.82±0.78)
250 nm	14.20 (14.09±0.25)	0.965 (0.965±0. 001)	0.592 (0.591±0.004)	8.11 (8.04±0.10)	13.96	1046.0 (1031.1±68.3)	10.5 (10.4±0.15)
300 nm	14.60 (14.12±0.23)	0.972 (0.965±0. 004)	0.578 (0.574±0.006)	8.20 (7.82±0.21)	14.03	919.5 (840.2±77.1)	11.6 (11.4±0.33)

(a) Average of 8 devices.

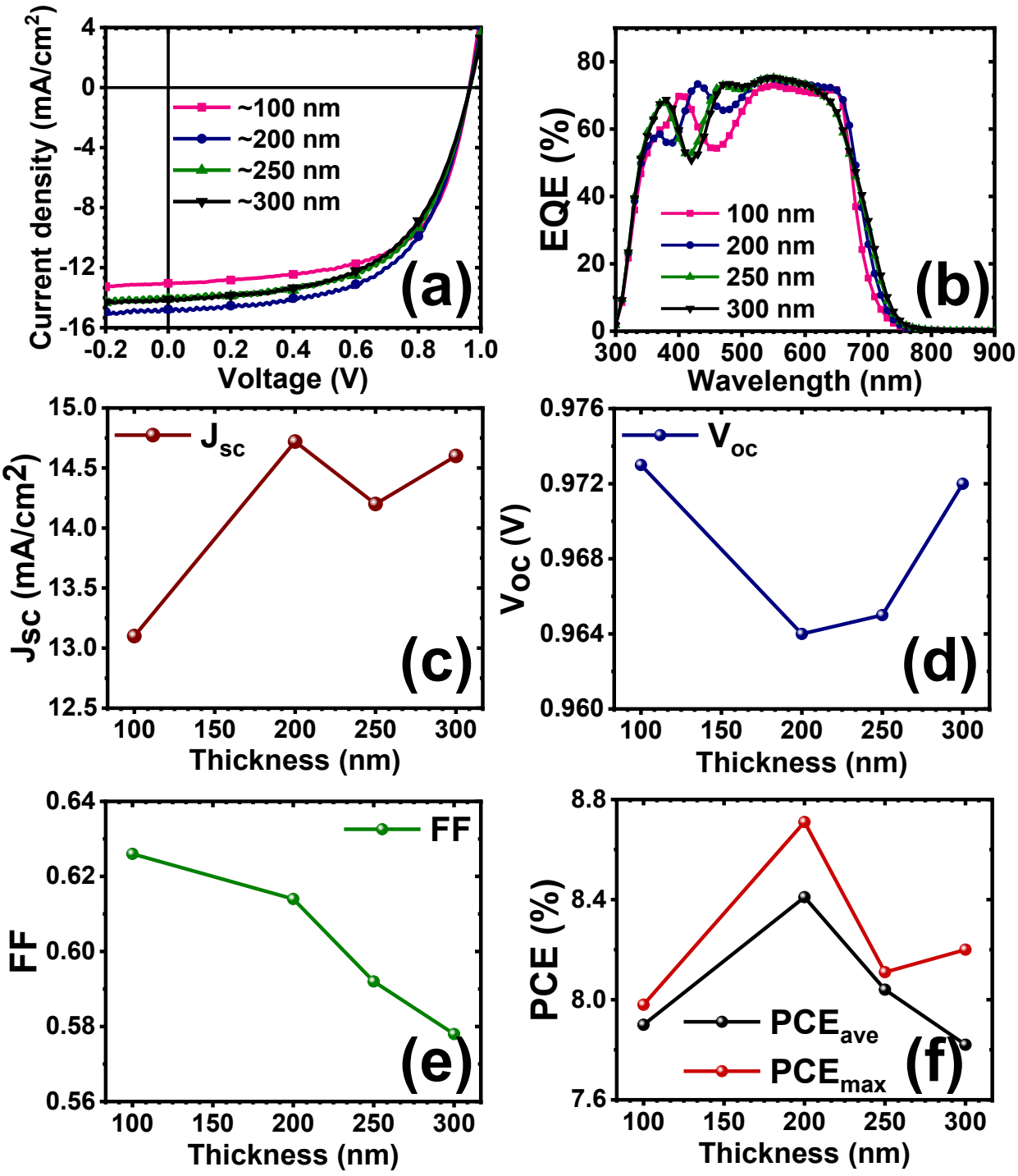

Figure 3. The optimized PM6:PNDIS devices processed from CB:2-MeTHF at various active layer thicknesses: (a) *J-V* curves; (b) EQE spectra; (c-f) J_{sc}, V_{oc}, FF, and PCE as a function of the active layer thickness.

The effect of fluorination of the donor polymer on optical bandgap energy loss ($E_{loss} = E_g^{opt} - eV_{oc}$) can be examined by considering the present results on PM6:PNDIBS and PM6:PNDIS in comparison to prior results on the non-fluorinated donor polymer PBDB-T.[12] From the E_g^{opt} values for PM6:PNDIS (1.67 eV) and PM6:PNDIBS (1.40 eV) blends and the observed V_{oc} values (Table 2), we obtain E_{loss} values of 0.70 eV for PM6:PNDIS and 0.475 eV for PM6:PNDIBS all-PSCs. Although the fluorinated donor polymer leads to a slight reduction (0.14 eV) from the PBDB-T blend, the observed E_{loss} for PM6:PNDIS is still quite large.[55, 56] The PNDIBS all-PSCs based on the non-fluorinated PBDB-T were found to combine E_{loss} of 0.55 eV with a moderate PCE of 7.9%. Thus, although fluorination results in the expected reduction in E_{loss} and enhancement of V_{oc} in PM6:PNDIBS, there is simultaneously an unexpected dramatic reduction in the photovoltaic efficiency from 7.9% to 3.1%. The possible sources of this unexpected huge effect of fluorination of the donor polymer on the performance of all-PSCs include blend morphology, blend photophysics, and charge transport, which will be examined later.

The EQE spectra of the optimized PM6:PNDIS and PM6:PNDIBS devices processed from CB as well as those processed from CB:2-MeTHF at various thicknesses are shown in Figure 2b and Figure 3b, respectively. The photo-response of PM6:PNDIS devices spanned from 740 nm to 300 nm and rose to a maximum EQE of 82% in the 540 – 590 nm region (Figure 2b). Although it covers a much broader range from 300 nm to 840 nm, the EQE spectrum of the optimal PM6:PNDIBS devices showed much lower EQE values almost across the entire spectrum with a maximum of 37% in the 520 – 570 nm region (Figure 2b). The broad photo-response over the entire ranges 300 – 840 nm for PM6:PNDIBS and 300 – 740 nm for PM6:PNDIS blends indicates efficient photoinduced electron and hole transfer.[57] In the case of PM6:PNDIS devices processed from CB:2-MeTHF co-solvent at various active layer thicknesses (Figure 3b), they showed lower

maximum EQE values of around 72 – 75% at 540 – 550 nm compared to those processed from CB. However, CB:2-MeTHF processed devices exhibited flatter EQE responses over a broad range from 450 nm to 650 nm (Figure 3b) and thus resulted in a slightly higher J_{sc} as observed in Table 2. The variations of the EQE spectra at certain wavelengths with increasing active layer thickness have been observed in prior reports ranging from fullerene-based devices to all-polymer solar cells and non-fullerene organic solar cells;[58-62] these variations can be rationalized by the inhomogeneous blend composition distribution in thicker films and optical interferences.[63-65] The corresponding photocurrent obtained from integration of the EQE spectra for PM6:PNDIS and PM6:PNDIBS blends were 13.25 mA/cm^2 and 6.52 mA/cm^2, respectively, which matched well with the values obtained from the *J-V* measurement (Table 1) within 2-4% error. The calculated J_{sc} from the EQE spectra of PM6:PNDIS based devices fabricated from CB:2-MeTHF co-solvents at various thicknesses were similarly in good agreement with the *J-V* measurements.

Charge Photogeneration and Charge Recombination. To elucidate the striking difference between the photovoltaic performance of PM6:PNDIS and PM6:PNDBS devices, the photoinduced charge generation rate and charge collection behavior of the optimized devices were characterized by measuring the photocurrent current ($J_{ph} = J_{illuminated} - J_{dark}$) as a function of effective voltage ($V_{eff} = V_{bias} - V_{applied}$). As shown in Figure 4a, the optimized PM6:PNDIS devices exhibited a field-independent charge photogeneration rate beyond 0.5V, which is consistent with previously observed systems that have FF higher than 0.65.[66-68] This result suggests that nearly all generated excitons effectively diffused to the donor/acceptor interface to form exciplexes[69] and instantaneously dissociated into free charges that are collected at the two electrodes and thereby effectively suppressing geminate recombination.[66] In contrast, the PM6:PNDIBS devices exhibited increasing photocurrent with increasing electric field, suggesting significant electron-

hole pair recombination. As a result, the charge photogeneration rate of PM6:PNDIS (8.58 x 10^{27} $m^{-3}s^{-1}$) was found to be 1.3-fold higher than that of PM6:PNDIBS (6.40 x 10^{27} $m^{-3}s^{-1}$). The charge collection probability (*P(E,T)*) at short-circuit condition was also calculated to be 99.1% and 65.5% for PM6:PNDIS and PM6:PNDIBS, respectively. The superior and near unity *P(E,T)* observed in PM6:PNDIS devices suggest that almost all dissociated charges were collected at the two electrodes, which is in agreement with the high J_{sc} and FF.

We also performed charge recombination analysis by characterizing the light-intensity dependence of J_{sc} and V_{oc}. The relationship between J_{sc} and the incident light intensity (P_{light}) can be generally described as $J_{sc} \propto P_{light}^{\alpha}$, where α represents the degree of bimolecular recombination.[66, 67] The value of α for the optimized PM6:PNDIBS blends (α = 0.95) deviated slightly from unity as shown in Figure 4b suggesting that some degree of bimolecular recombination can be expected in these devices. However, the optimized PM6:PNDIS devices exhibited an α value of 1.01 indicative of highly suppressed bimolecular recombination, which is in good accordance with the observed higher J_{sc} and FF. The relationship between V_{oc} and P_{light} which can be generalized as $V_{oc} \propto s \times \ln(P_{light})$. The proportional coefficient s usually varies between 1 and 2 representing either a dominating bimolecular recombination (s = 1kT/q) or a preferable trap-assisted recombination (s = 2kT/q).[66] The data in Figure 4c show that PM6:PNDIS devices follow a trap-assisted recombination (s = 1.48 kT/q) whereas PM6:PNDIBS devices have a s of 1.21kT/q which suggests that bimolecular recombination governs its charge recombination kinetics.

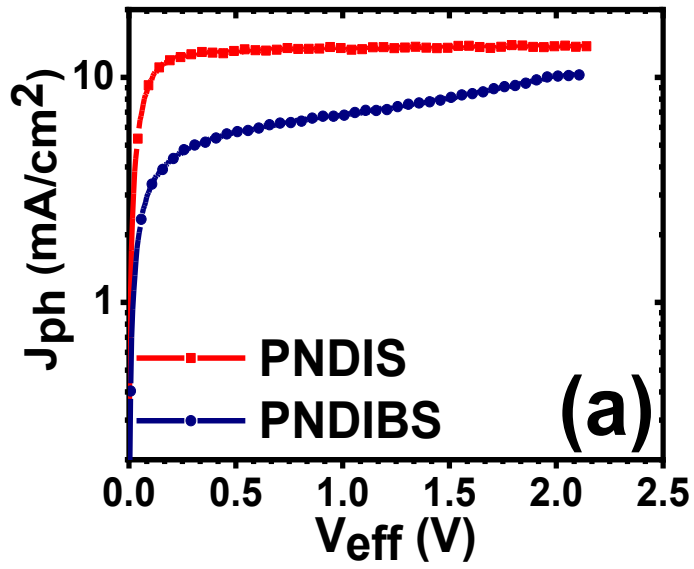
10
1
J_{ph} (mA/cm^2)
PNDIS
PNDIBS
(a)
0.0
0.5
1.0
1.5
2.0
2.5
V_{eff} (V)

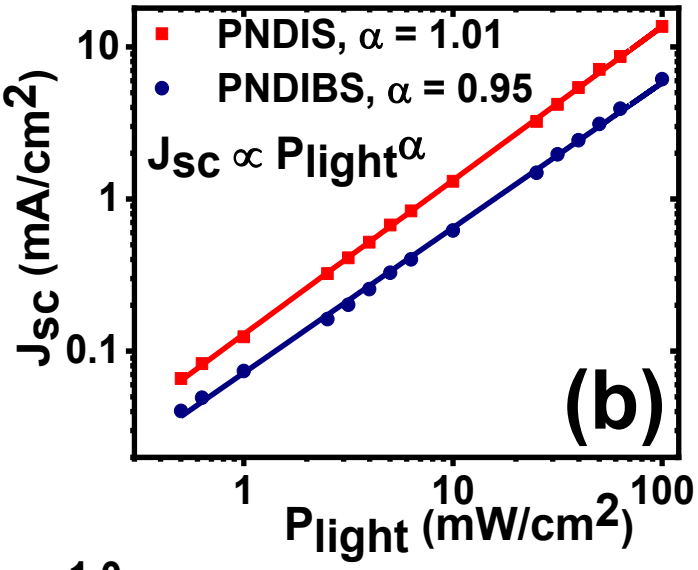
PNDIS, α = 1.01
PNDIBS, α = 0.95
$J_{sc} \propto P_{light}^{\alpha}$
10
1
0.1
J_{sc} (mA/cm^2)
(b)
1
10
100
P_{light} (mW/cm^2)

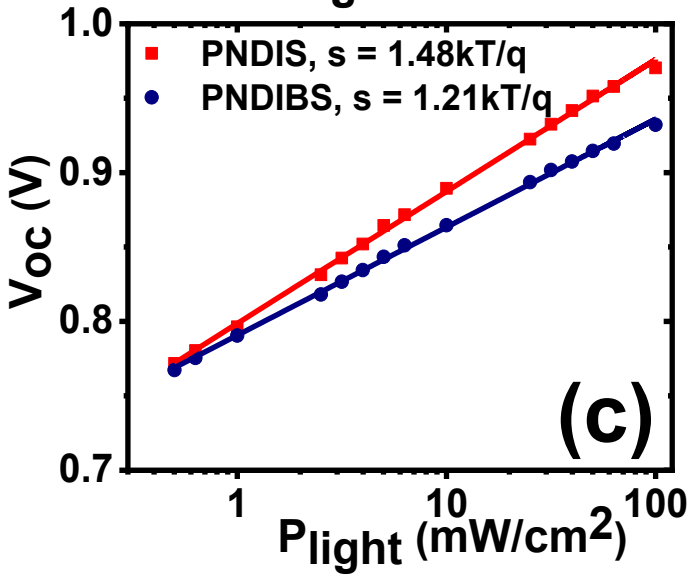
PNDIS, s = 1.48kT/q
PNDIBS, s = 1.21kT/q
1.0
0.9
0.8
0.7
V_{oc} (V)
(c)
1
10
100
P_{light} (mW/cm^2)

Figure 4. (a) J_{ph}-V_{eff} curves, (b) J_{sc} dependency on incident light intensity , and (c) V_{oc} dependency on incident light intensity for the optimized PM6:PNDIS and PM6:PNDIBS blend devices. All blends were processed under optimized conditions from chlorobenzene.

Charge Transport Properties. We investigated the charge transport properties of PM6:PNDIS and PM6:PNDIBS blend films and neat films of the individual components by the space-charge limited current (SCLC) method. Single-carrier devices were fabricated in the following device architectures: ITO/PEDOT:PSS/Blend/MoO_3/Ag for hole-only devices and ITO/ZnO/PEI/Blend/LiF/Al for electron-only devices. The resulting *J-V* curves were fitted to the Mott-Gurney equation to extract the charge carrier mobilities. The *J-V* curves and their fit lines for neat and blend films are shown in Figures S6 and S7, respectively, while the carrier mobilities are summarized in Table 3.

The neat films of the donor polymer PM6 showed a relatively high hole mobility (μ_h) of 1.2 x 10^{-4} cm^2/Vs, which is in agreement with prior reports.[21, 40, 41] The electron mobility (μ_e) of neat films of PNDIS and PNDIBS was found to be 1.24 x 10^{-4} cm^2/Vs and 2.13 x 10^{-4} cm^2/Vs, respectively, which are also in agreement with reported values.[8, 12, 20, 49] The slightly higher electron mobility in neat PNDIBS films can be explained by its higher crystallinity compared to PNDIS as evidenced by GIWAXS and AFM results to be discussed below. In PM6:PNDIBS blend films, μ_h and μ_e were 1.98 x 10^{-4} cm^2/Vs and 7.28 x 10^{-5} cm^2/Vs, respectively. Compared to the PM6:PNDIBS blends, the hole mobility of the PM6:PNDIS blends increased by 1.6-fold to 3.25 x 10^{-4} cm^2/Vs; however, the electron mobility was lowered to 1.89 x 10^{-5} cm^2/Vs. The asymmetric charge transport observed in PM6:PNDIS indicated that further optimization to improve the device performance is feasible.

Effects of the co-solvent processing on the bulk charge carrier mobilities of PM6:PNDIS blends were also examined. The μ_h was found to increase from 3.25 x 10^{-4} cm^2/Vs when processed from CB to 4.11 x 10^{-4} cm^2/Vs when processed from the CB:2-MeTHF co-solvents. Similarly, the bulk μ_e for blends processed from CB:2-MeTHF was significantly increased by almost an order of magnitude to 1.36 x 10^{-4} cm^2/Vs. As explained earlier, the solubility differences of the blend components in the co-solvent system (CB:2-MeTHF) and the boiling point differences of the two solvents enable independent tuning of the aggregation rates and thereby, higher domain purity can be achieved as evidenced by the increased surface roughness observed in AFM images (Figure S5). Thus, the observed higher hole and electron mobilities for blends processed from the CB:2-MeTHF co-solvent can be rationalized by the optimal blend morphology featuring higher domain purity and optimal domain sizes, which is consistent to previous study demonstrating enhanced charge carrier mobility for blends processed from 2-MeTHF.[70] Furthermore, the observed higher hole and electron mobilities for blends processed via the CB:2-MeTHF co-solvent technique are in good agreement with the efficient photovoltaic device performance even for thick film active layers.

Table 3. SCLC Mobilities of Neat Films of PM6, PNDIS, and PNDIBS and Blend Films of PM6:PNDIS and PM6:PNDIBS. All Active Layers were Processed at Optimal Conditions.

Neat or Blend Films	μ_e (cm^2/Vs)	μ_h (cm^2/Vs)	μ_h / μ_e
PM6	-	1.20 x 10^{-4}	-
PNDIS	1.24 x 10^{-4}	-	-
PNDIBS	2.13 x 10^{-4}	-	-
PM6:PNDIS (CB)	1.89 x 10^{-5}	3.25 x 10^{-4}	17.2
PM6:PNDIBS (CB)	7.28 x 10^{-5}	1.98 x 10^{-4}	2.72

PM6:PNDIS (CB:2-MeTHF)	1.36×10^{-4}	4.11×10^{-4}	3.03

Vertical Phase Stratification. Interestingly, we found that the electron mobility of PM6:PNDIS blends varied by orders of magnitude depending on the direction of bias voltage. As shown in Figure 5a, the PM6:PNDIS electron-only devices exhibited asymmetric *J-V* behavior under positive and negative bias, which was not observed in the PM6:PNDIBS devices (Figures 5b and 5d). Observation of such asymmetric electron injection behavior has previously been attributed to the vertical phase stratification of the active layer.[71] In the present case, vertical phase segregation in the blend means that PNDIS was buried near the ZnO/PEI interface and PM6 accumulated near the top surfaces, and thus, forming a significant energetic barrier at the Al electrode and inhibiting electron injection into the active layer (Figure 5c).[71]

Additional characterizations using time-of-flight secondary ion mass spectroscopy (TOF-SIMs) and contact angle measurements further confirmed a greater degree of vertical phase separation in the PM6:PNDIS blends. Figure 6 shows the vertical composition distribution of F^- and CN^-, which are representative of the donor polymer (PM6) and the acceptor polymers (PNDIS and PNDIBS), respectively, from the top air surface to the bottom ZnO/PEI interface. The profile of CN^- in the PM6:PNDIS blends clearly showed a gradient with increasing concentration towards the ZnO/PEI interface (Figure 6a), whereas the concentration of CN^- in the PM6:PNDIBS blends remained constant across the active layer thickness (Figure 6b). Moreover, the profile of F^- in the PM6:PNDIS blends exhibited a sharp decline as $t/t_{active\ layer}$ approached unity (Figure 6a), which indicated that the donor polymer PM6 was depleted at the cathode interface. On the other hand, as shown in Figure 6b, the concentration of F^- in the PM6:PNDIBS blends stayed nearly unchanged throughout the active layer thickness. These results strongly suggest that a greater degree of vertical phase separation exists in the PM6:PNDIS blends, where the acceptor polymer

concentration gradually increases and accumulates at the cathode interface. This result is in agreement with the asymmetric *J-V* behavior under different voltage bias direction.

The surface energy of the donor polymer and the acceptor polymers and the Flory-Huggins interaction parameters of the respective blends were investigated and are summarized in Table S5 via contact angle measurements on their neat films with diiodomethane and water as the wetting liquids shown in Figure S8. As summarized in Table S5, the surface energy (γ) of the donor polymer PM6 was found to be 37.05 mN/m which is comparable to that of PNDIBS (γ = 37.46 mN/m), suggesting a homogenous blend distribution across the active layer thickness in very good agreement with the *J-V* behaviors and the TOF-SIMs analysis. The estimated Flory-Huggins interaction parameter was also calculated based on the empirical equation $\chi_{donor,acceptor} = K\left(\sqrt{\gamma_{donor}} - \sqrt{\gamma_{acceptor}}\right)^2$, where K is a constant. A small $\chi_{\text{donor, acceptor}}$ value means a highly miscible blends while a large $\chi_{\text{donor, acceptor}}$ value suggests phase separation in blend films.[27] The $\chi_{\text{donor, acceptor}}$ value for the PM6:PNDIBS blends was found to be extremely low at 0.00113K (Table S5) suggesting excessively miscible blends, which would be detrimental to domain purity. As a result, the PM6:PNDIBS devices suffered from poor charge photogeneration and significant charge recombination. On the other hand, the higher surface energy of PNDIS (γ = 39.08 mN/m) (Table S5) compared to PM6 indicated that the donor polymer PM6 would migrate towards the air interface while the acceptor polymer PNDIS would be preferentially buried at the bottom interface.[72] The $\chi_{\text{donor, acceptor}}$ value of the PM6:PNDIS blends increased over 20-fold compared to that of the PM6:PNDIBS blends, suggesting that optimal blend miscibility was achieved and thereby, enhancing the domain purity. The results of these characterization techniques collectively show that there is a greater degree of vertical phase separation and better domain purity in the PM6:PNDIS blends, which is beneficial for charge extraction and suppression of bimolecular

charge recombination. This result is in excellent agreement with the near unity charge collection probability and the negligible charge recombination, leading to the observed higher J_{sc} and FF in the PM6:PNDIS all-PSCs.[71, 73, 74]

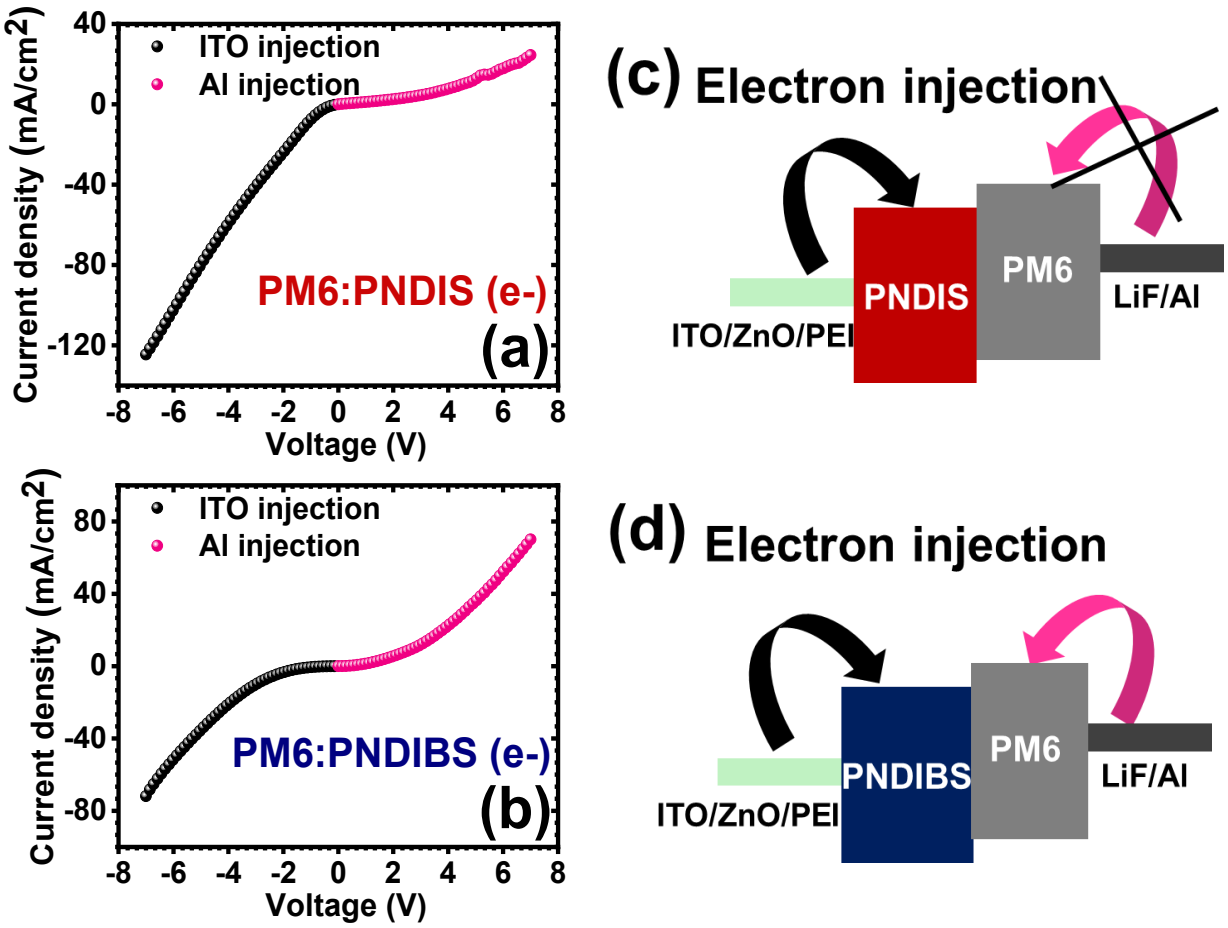

Figure 5. (a) *J-V* curves for electron-only SCLC PM6:PNDIS devices under positive and negative bias. (b) *J-V* curves for electron-only SCLC PM6:PNDIBS devices under positive and negative bias. (c) Schematics for electron injection in PM6:PNDIS devices under positive and negative bias. (d) Schematics for electron injection in PM6:PNDIBS devices under positive and negative bias. All blends were processed under optimized conditions from chlorobenzene.

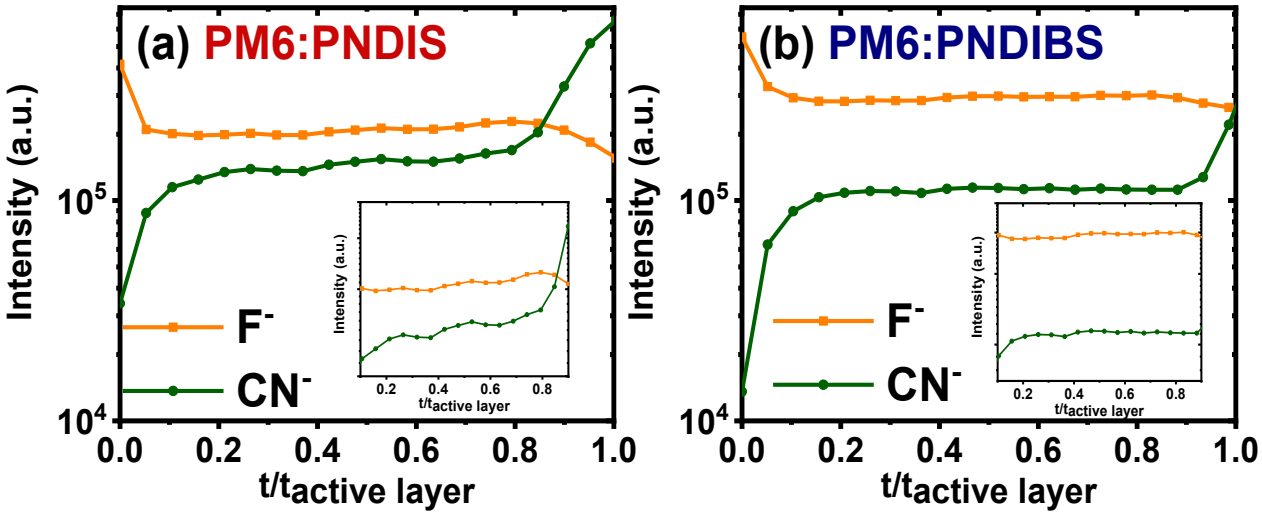

Figure 6. (a) TOF-SIM profiles of F^- and CN^- for PM6:PNDIS devices across the active layer thickness. (b) TOF-SIM profiles of F^- and CN^- for PM6:PNDIBS devices across the active layer thickness. All blends were processed under the optimized conditions from chlorobenzene.

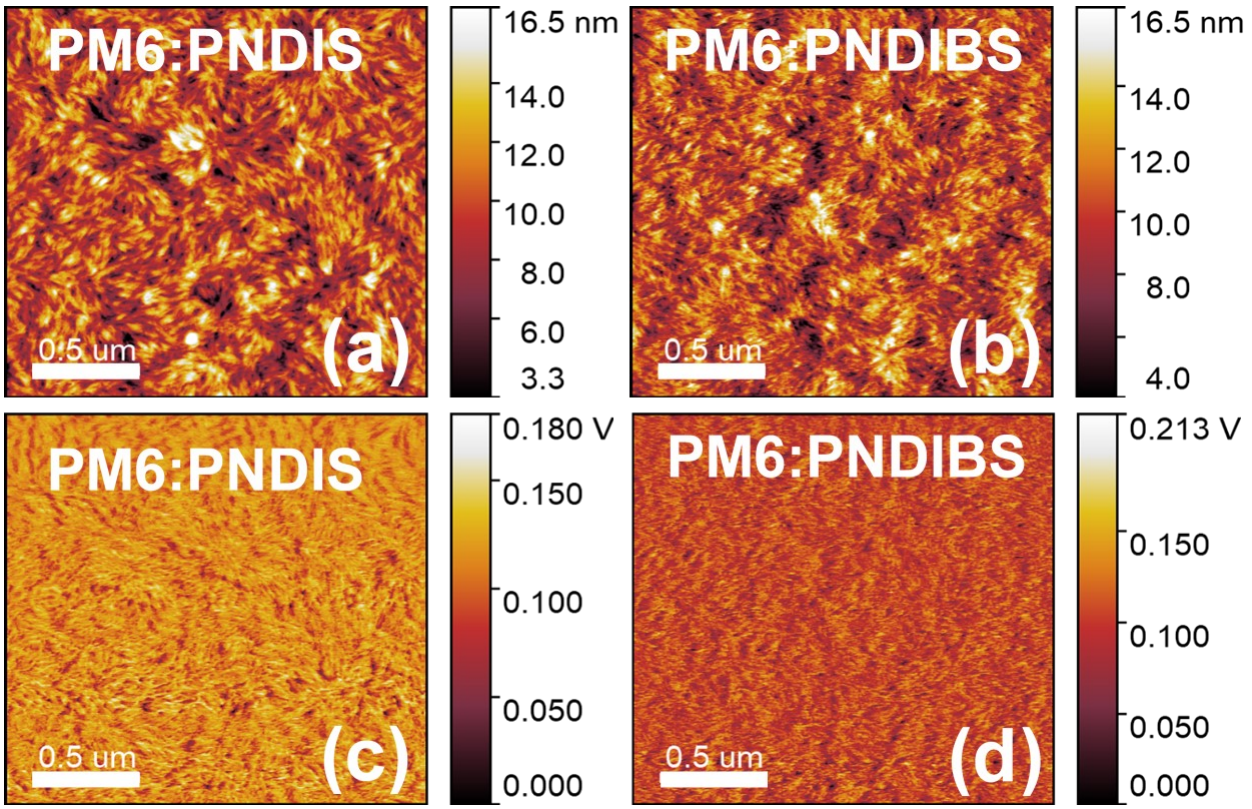

Figure 7. AFM height (a, b) and phase (c, d) images (2 μm x 2 μm) of the surfaces of PM6:PNDIS (a, c) and PM6:PNDIBS (b, d) blend films processed from optimized conditions in chlorobenzene. The scale bars are 500 nm.

Surface and Bulk Morphology. The surface morphology of neat and blend films was investigated by atomic force microscopy (AFM) imaging (Figures 7 and S9). Although neat films of both of the acceptors showed relatively smooth surfaces (R_q ~ 1.1 nm), neat films of PNDIS showed a rather amorphous surface with no distinct features while neat films of PNDIBS exhibited homogenous fibrillar structures indicative of the highly crystalline nature of this polymer (Figure S9).[12] Despite the clear differences in the surface morphology of neat PNDIS and PNDIBS films, their blend films (PM6:PNDIS and PM6:PNDIBS) showed similar morphology with distinctive needle-like features with comparable surface roughness (R_q ~ 2 nm) and domain size (~ 22 – 25 nm) (Figure 7).

To gain more insights into the bulk morphology of the blend films, 2D-grazing incident wide-angle X-ray scattering (2D-GIWAXS) measurements were carried out on both the neat films and blend films. The 2D-GIWAXS images and the corresponding line cuts for the neat donor and acceptor films are presented in Figure S10, while those of the blend films are shown in Figure 8. The peak positions as well as the *d*-spacings for both the neat and blend films are summarized in Table S6. The neat films of donor polymer PM6 exhibit distinct (100) diffraction peaks in both the in-plane (IP) and the out-of-plane (OOP) directions at around 0.30 $Å^{-1}$ and 0.33 $Å^{-1}$ (Figures S10d and S10e), which corresponds to a *d*-spacing of 19.04 – 20.94 Å, respectively (Table S6). The (010) peaks were also present in both IP and OOP directions of neat PM6 films, centering at 1.68 – 1.71 $Å^{-1}$ (Figure S10d and S10e) with a *d*-spacing of 3.67 – 3.74 Å. The pronounced (100) and (010) diffraction peaks in both the IP and the OOP directions indicate the coexistence of both *face-*

on and *edge-on* molecular orientations in neat PM6 films, which is consistent with previous reports.[40]

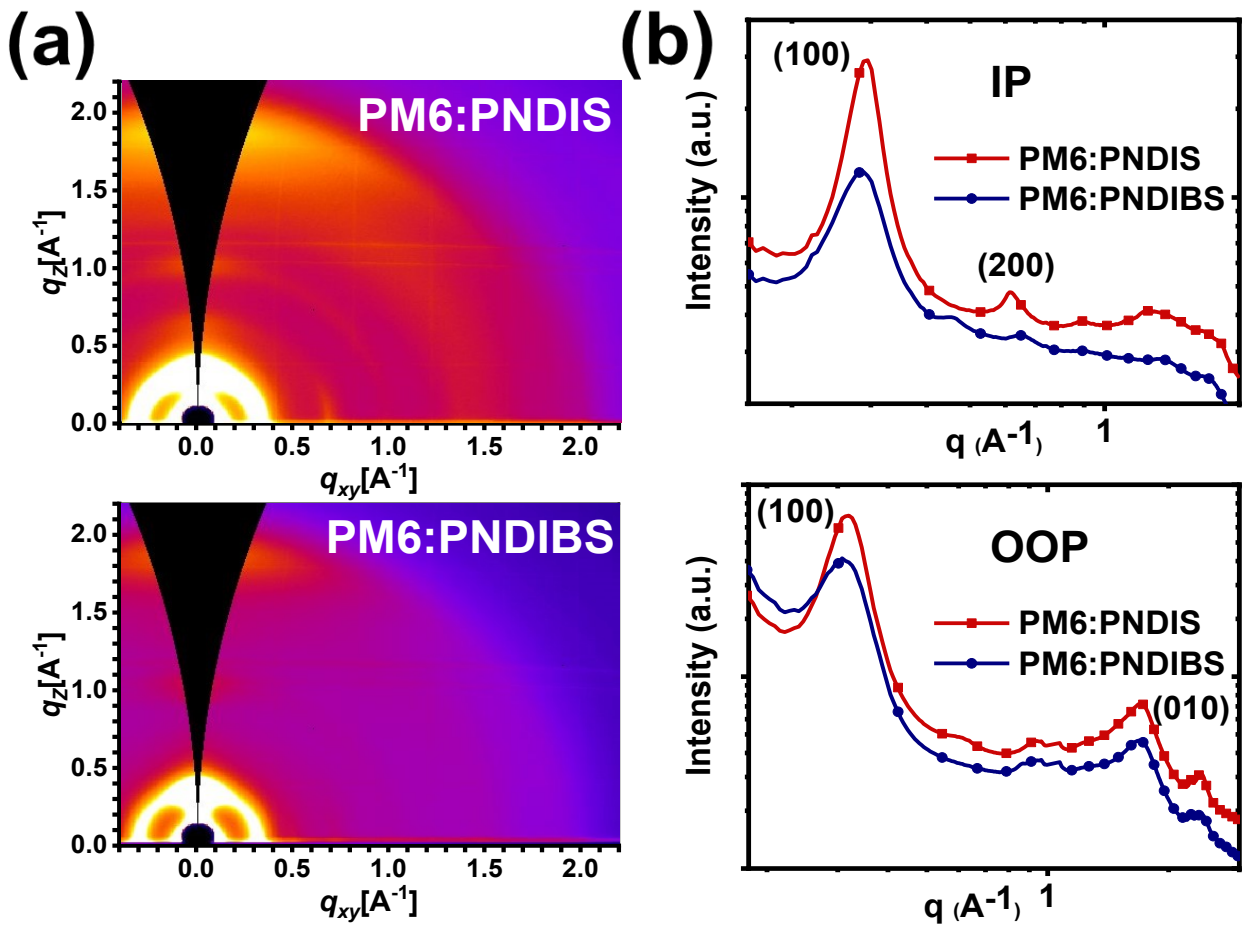

Figure 8. 2D-GIWAXS patterns of (a) PM6:PNDIS blend film and PM6:PNDIBS blend film. (b) In-plane (IP) and out-of-plane (OOP) line-cuts GIWAXS patterns for PM6:PNDIS and PM6:PNDIBS blend films.

Neat films of PNDIS and PNDIBS had intense (100) diffraction peaks in the IP direction at q_{xy} of 0.29 and 0.26 Å^{-1}, respectively, corresponding to *d*-spacings of 21.67 Å and 24.17 Å (Table S6). The larger lamellar distance observed in neat PNDIBS films can be attributed to its longer 2-octyldodecyl side chains relative to the 2-hexyldecyl side chains in PNDIS. These lamellar packing

distances in both PNDIS and PNDIBS are significantly shorter than expected from their alkyl chain lengths, clearly indicating interdigitation of the alkyl side chains between adjacent polymer backbones.[75] Higher order reflections of the lamellar packings were also present in the neat acceptor polymer films as evidenced by the (200) peaks in the IP direction (Figure S10b). Pronounced (010) peaks in the OOP direction were also observed in both PNDIS and PNDIBS neat films (q_z = 1.57 – 1.58 $Å^{-1}$) with a π- π stacking distance of 3.98 – 4.00 Å (Table S6). Compared to PNDIS, PNDIBS exhibited slightly broader and more intense (100) and (010) peaks in the IP and OOP directions, respectively. While PNDIBS had a rather weak (100) peak in the OOP direction, PNDIS exhibited a more pronounced (100) diffraction peak at 0.29 $Å^{-1}$. These observations collectively suggested that PNDIBS predominantly adopted *face-on* molecular orientation while PNDIS exhibited mixed *face-on* and *edge-on* populations.

In the blend films, the (100) peaks in the OOP direction, which mainly originated from the PM6 donor polymer, became sharper, more intense, and shifted to a lower q_z value (q_z = 0.31 – 0.32 $Å^{-1}$) that lied between the q_z values of the donor and the acceptor polymers (Table S6); thereby suggesting well-mixed blends. Pronounced (100) diffraction peaks in the IP direction were also observed (q_{xy} = 0.29 $Å^{-1}$) in both PM6:PDNIS and PM6:PNDIBS blends. Moreover, the lamellar *face-on* (200) ordering peaks were preserved in PM6:PNDIS blend but disappeared in PM6:PNDIBS blend (Figure 8b). The crystal coherence length (L_c) calculated using Scherrer equation was found to be 10.5 nm and 8.1 nm for PM6:PNDIS and PM6:PNDIBS blends, respectively. The higher L_c values and the presence of highly ordered lamellar peaks observed in PM6:PDNIS blends indicated that PNDIS retained its crystallinity upon blending with the donor polymer PM6 while the crystallinity of PNDIBS decreased in blend films. Moreover, the L_c of PM6:PNDIS blends (10.5 nm) is comparable to the typical exciton diffusion length[76, 77] enabling

highly efficient exciton diffusion and charge photogeneration as explained earlier. Compared to the neat acceptor polymer films, the (010) peaks in the OOP direction shifted to higher q_z values of 1.69 $Å^{-1}$ for PM6:PNDIBS blends and 1.71 $Å^{-1}$ for PM6:PNDIS blends. The observation of sharp and intense (100) and (010) peaks in the IP and OOP directions, respectively, in the PM6:PNDIS blends clearly show that the polymer chains exhibit preferential *face-on* molecular orientation in the blends, which is favorable for charge transport across the electrical contacts.

CONCLUSIONS

We have investigated how a fluorinated donor polymer (PM6) influences the photovoltaic properties, blend morphology, and blend photophysics of all-PSCs based on NDI-arylene copolymer acceptors. We found that pairing of PM6 respectively with PNDIS and PNDIBS led to dramatically different photovoltaic, blend morphology, and blend photophysics results. PM6:PNDIS all-PSCs combined the expected enhancement in V_{oc} (0.967 V) with high fill factor (0.70) to enable 9.1% PCE due to the vertical phase stratification and predominant *face-on* molecular orientations in the blend nanomorphology. In addition, the blend photophysics of PM6:PNDIS featured high charge photogeneration rate, strongly suppressed geminate and bimolecular recombinations, and near unity charge collection probability. However, despite a favorable low optical bandgap energy loss (0.475 eV) and enhanced V_{oc} (0.925 V) in PM6:PNDIBS all-PSCs, compared to similar blends of the non-fluorinated PBDB-T, they showed poor performance (3.1% PCE) that originated from bulk phase separation with both *face-on* and *edge-on* molecular orientations, poor charge collection probability (66%) and high electron-hole recombination rate. These results show that in addition to the expected enhancement of V_{oc}, a fluorinated polymer in all-PSCs can also dramatically influence the blend morphology and blend photophysics with consequent negative or positive impact on the photovoltaic performance. The

results also demonstrate that PM6:PNDIS all-PSCs are promising efficient devices that are robust to various processing methods and to active layer thicknesses of up to 300 nm.

ASSOCIATED CONTENT

Supporting Information.

The Supporting Information is available free of charge on the ACS Publications website at .

Additional characterization data: UV−vis, *J-V* curves measured by SCLC and the corresponding fits, AFM images of neat donor polymer and acceptor polymer films, Contact angle measurements, 2D-GIWAXS images of neat donor polymer and acceptor polymer films with 1D line cuts, and details of device optimization. (PDF)

AUTHOR INFORMATION

Corresponding Author

*Email: jenekhe@u.washington.edu

Author Contributions

The manuscript was written through contributions of all authors. All authors have given approval to the final version of the manuscript.

Notes

The authors declare no competing financial interest.

ACKNOWLEDGMENT

This work was supported by the NSF (DMR-1708450) and the Office of Naval Research (N00014-17-1-2203). D.K.T. gratefully acknowledges the Clean Energy Institute Fellowship. The

synchrotron radiation-based 2D-GIWAXS experiments were performed at the BL46XU of SPring-8 with the approval of the Japan Synchrotron Radiation Research Institute (JASRI) (Proposal Nos. 2018B1772).

REFERENCES

1. Lee, C.; Lee, S.; Kim, G.-U.; Lee, W.; Kim, B. J. "Recent Advances, Design Guidelines, and Prospects of All-Polymer Solar Cells." *Chem. Rev.* **2019,** *119* (13), 8028-8086.

2. Wang, G.; Melkonyan, F. S.; Facchetti, A.; Marks, T. J. "All-Polymer Solar Cells: Recent Progress, Challenges, and Prospects." *Angew. Chem. Int. Ed.* **2019,** *58* (13), 4129-4142.

3. Genene, Z.; Mammo, W.; Wang, E.; Andersson, M. R. "Recent Advances in n-Type Polymers for All-Polymer Solar Cells." *Adv. Mater.* **2019,** *31* (22), 1807275.

4. Benten, H.; Mori, D.; Ohkita, H.; Ito, S. "Recent Research Progress of Polymer Donor/Polymer Acceptor Blend Solar Cells." *J. Mater. Chem. A* **2016,** *4* (15), 5340-5365.

5. Yuan, J.; Zhang, Y.; Zhou, L.; Zhang, G.; Yip, H.-L.; Lau, T.-K.; Lu, X.; Zhu, C.; Peng, H.; Johnson, P. A.; Leclerc, M.; Cao, Y.; Ulanski, J.; Li, Y.; Zou, Y. "Single-Junction Organic Solar Cell with over 15% Efficiency Using Fused-Ring Acceptor with Electron-Deficient Core." *Joule* **2019,** *3* (4), 1140-1151.

6. Cui, Y.; Yao, H.; Zhang, J.; Zhang, T.; Wang, Y.; Hong, L.; Xian, K.; Xu, B.; Zhang, S.; Peng, J.; Wei, Z.; Gao, F.; Hou, J. "Over 16% Efficiency Organic Photovoltaic Cells Enabled by A Chlorinated Acceptor With Increased Open-Circuit Voltages." *Nat. Commun.* **2019,** *10* (1), 2515.

7. Hwang, Y.-J.; Ren, G.; Murari, N. M.; Jenekhe, S. A. "n-Type Naphthalene Diimide–Biselenophene Copolymer for All-Polymer Bulk Heterojunction Solar Cells." *Macromolecules* **2012,** *45* (22), 9056-9062.

8. Hwang, Y.-J.; Courtright, B. A. E.; Ferreira, A. S.; Tolbert, S. H.; Jenekhe, S. A. "7.7% Efficient All-Polymer Solar Cells." *Adv. Mater.* **2015,** *27* (31), 4578-4584.

9. Zhang, Y.; Xu, Y.; Ford, M. J.; Li, F.; Sun, J.; Ling, X.; Wang, Y.; Gu, J.; Yuan, J.; Ma, W. "Thermally Stable All-Polymer Solar Cells with High Tolerance on Blend Ratios." *Adv. Energy Mater.* **2018,** *8* (18), 1800029.

10. Deshmukh, K. D.; Matsidik, R.; Prasad, S. K. K.; Connal, L. A.; Liu, A. C. Y.; Gann, E.; Thomsen, L.; Hodgkiss, J. M.; Sommer, M.; McNeill, C. R. "Tuning the Molecular Weight of the Electron Accepting Polymer in All-Polymer Solar Cells: Impact on Morphology and Charge Generation." *Adv. Funct. Mater.* **2018,** *28* (18), 1707185.

11. Kim, T.; Kim, J.-H.; Kang, T. E.; Lee, C.; Kang, H.; Shin, M.; Wang, C.; Ma, B.; Jeong, U.; Kim, T.-S.; Kim, B. J. "Flexible, Highly Efficient All-Polymer Solar Cells." *Nat. Commun.* **2015,** *6*, 8547.

12. Kolhe, N. B.; Lee, H.; Kuzuhara, D.; Yoshimoto, N.; Koganezawa, T.; Jenekhe, S. A. "All-Polymer Solar Cells with 9.4% Efficiency from Naphthalene Diimide-Biselenophene Copolymer Acceptor." *Chem. Mater.* **2018,** *30* (18), 6540-6548.

13. Wu, Y.; Schneider, S.; Walter, C.; Chowdhury, A. H.; Bahrami, B.; Wu, H.-C.; Qiao, Q.; Toney, M. F.; Bao, Z. "Fine-Tuning Semiconducting Polymer Self-Aggregation and

Crystallinity Enables Optimal Morphology and High-Performance Printed All-Polymer Solar Cells." *J. Am. Chem. Soc.* **2019,** *142* (1), 392-406.

14. Li, Z.; Xu, X.; Zhang, W.; Meng, X.; Ma, W.; Yartsev, A.; Inganäs, O.; Andersson, M. R.; Janssen, R. A. J.; Wang, E. "High Performance All-Polymer Solar Cells by Synergistic Effects of Fine-Tuned Crystallinity and Solvent Annealing." *J. Am. Chem. Soc.* **2016,** *138* (34), 10935-10944.

15. Xu, X.; Li, Z.; Zhang, W.; Meng, X.; Zou, X.; Di Carlo Rasi, D.; Ma, W.; Yartsev, A.; Andersson, M. R.; Janssen, R. A. J.; Wang, E. "8.0% Efficient All-Polymer Solar Cells with High Photovoltage of 1.1 V and Internal Quantum Efficiency near Unity." *Adv. Energy Mater.* **2018,** *8* (1), 1700908.

16. Fan, B.; Ying, L.; Zhu, P.; Pan, F.; Liu, F.; Chen, J.; Huang, F.; Cao, Y. "All-Polymer Solar Cells Based on a Conjugated Polymer Containing Siloxane-Functionalized Side Chains with Efficiency over 10%." *Adv. Mater.* **2017,** *29* (47), 1703906.

17. Gao, L.; Zhang, Z.-G.; Xue, L.; Min, J.; Zhang, J.; Wei, Z.; Li, Y. "All-Polymer Solar Cells Based on Absorption-Complementary Polymer Donor and Acceptor with High Power Conversion Efficiency of 8.27%." *Adv. Mater.* **2016,** *28* (9), 1884-1890.

18. Shi, G.; Yuan, J.; Huang, X.; Lu, Y.; Liu, Z.; Peng, J.; Ding, G.; Shi, S.; Sun, J.; Lu, K.; Wang, H.-Q.; Ma, W. "Combinative Effect of Additive and Thermal Annealing Processes Delivers High Efficiency All-Polymer Solar Cells." *J. Phys. Chem. C* **2015,** *119* (45), 25298-25306.

19. Robitaille, A.; Jenekhe, S. A.; Leclerc, M. "Poly(naphthalene diimide-alt-bithiophene) Prepared by Direct (Hetero)arylation Polymerization for Efficient All-Polymer Solar Cells." *Chem. Mater.* **2018,** *30* (15), 5353-5361.

20. Earmme, T.; Hwang, Y.-J.; Subramaniyan, S.; Jenekhe, S. A. "All-Polymer Bulk Heterojuction Solar Cells with 4.8% Efficiency Achieved by Solution Processing from a Co-Solvent." *Adv. Mater.* **2014,** *26* (35), 6080-6085.

21. Yao, H.; Bai, F.; Hu, H.; Arunagiri, L.; Zhang, J.; Chen, Y.; Yu, H.; Chen, S.; Liu, T.; Lai, J. Y. L.; Zou, Y.; Ade, H.; Yan, H. "Efficient All-Polymer Solar Cells based on a New Polymer Acceptor Achieving 10.3% Power Conversion Efficiency." *ACS Energy Lett.* **2019,** *4* (2), 417-422.

22. Kim, Y. J.; Ahn, S.; Wang, D. H.; Park, C. E. "A Mechanistic Understanding of a Binary Additive System to Synergistically Boost Efficiency in All-Polymer Solar Cells." *Sci. Rep.* **2015,** *5*, 18024.

23. Hwang, Y.-J.; Earmme, T.; Subramaniyan, S.; Jenekhe, S. A. "Side Chain Engineering of N-Type Conjugated Polymer Enhances Photocurrent and Efficiency of All-Polymer Solar Cells." *Chem. Commun.* **2014,** *50* (74), 10801-10804.

24. Lee, C.; Kang, H.; Lee, W.; Kim, T.; Kim, K.-H.; Woo, H. Y.; Wang, C.; Kim, B. J. "High-Performance All-Polymer Solar Cells Via Side-Chain Engineering of the Polymer Acceptor: The Importance of the Polymer Packing Structure and the Nanoscale Blend Morphology." *Adv. Mater.* **2015,** *27* (15), 2466-2471.

25. Lee, W.; Lee, C.; Yu, H.; Kim, D.-J.; Wang, C.; Woo, H. Y.; Oh, J. H.; Kim, B. J. "Side Chain Optimization of Naphthalenediimide-Bithiophene-Based Polymers to Enhance the Electron Mobility and the Performance in All-Polymer Solar Cells." *Adv. Funct. Mater.* **2016,** *26* (10), 1543-1553.

26. Hwang, Y.-J.; Earmme, T.; Courtright, B. A. E.; Eberle, F. N.; Jenekhe, S. A. "n-Type Semiconducting Naphthalene Diimide-Perylene Diimide Copolymers: Controlling Crystallinity, Blend Morphology, and Compatibility Toward High-Performance All-Polymer Solar Cells." *J. Am. Chem. Soc.* **2015,** *137* (13), 4424-4434.

27. Liu, X.; Zhang, C.; Duan, C.; Li, M.; Hu, Z.; Wang, J.; Liu, F.; Li, N.; Brabec, C. J.; Janssen, R. A. J.; Bazan, G. C.; Huang, F.; Cao, Y. "Morphology Optimization via Side Chain Engineering Enables All-Polymer Solar Cells with Excellent Fill Factor and Stability." *J. Am. Chem. Soc.* **2018,** *140* (28), 8934-8943.

28. Kolhe, N. B.; Tran, D. K.; Lee, H.; Kuzuhara, D.; Yoshimoto, N.; Koganezawa, T.; Jenekhe, S. A. "New Random Copolymer Acceptors Enable Additive-Free Processing of 10.1% Efficient All-Polymer Solar Cells with Near-Unity Internal Quantum Efficiency." *ACS Energy Lett.* **2019,** *4* (5), 1162-1170.

29. Xu, X.; Li, Z.; Wang, J.; Lin, B.; Ma, W.; Xia, Y.; Andersson, M. R.; Janssen, R. A. J.; Wang, E. "High-Performance All-Polymer Solar Cells Based on Fluorinated Naphthalene Diimide Acceptor Polymers with Fine-Tuned Crystallinity and Enhanced Dielectric Constants." *Nano Energy* **2018,** *45*, 368-379.

30. Li, W.; Ye, L.; Li, S.; Yao, H.; Ade, H.; Hou, J. "A High-Efficiency Organic Solar Cell Enabled by the Strong Intramolecular Electron Push-Pull Effect of the Nonfullerene Acceptor." *Adv. Mater.* **2018,** *30* (16), 1707170.

31. Zhao, W.; Li, S.; Yao, H.; Zhang, S.; Zhang, Y.; Yang, B.; Hou, J. "Molecular Optimization Enables over 13% Efficiency in Organic Solar Cells." *J. Am. Chem. Soc.* **2017,** *139* (21), 7148-7151.

32. Zhang, M.; Guo, X.; Zhang, S.; Hou, J. "Synergistic Effect of Fluorination on Molecular Energy Level Modulation in Highly Efficient Photovoltaic Polymers." *Adv. Mater.* **2014,** *26* (7), 1118-1123.

33. Deng, D.; Zhang, Y.; Zhang, J.; Wang, Z.; Zhu, L.; Fang, J.; Xia, B.; Wang, Z.; Lu, K.; Ma, W.; Wei, Z. "Fluorination-Enabled Optimal Morphology Leads to Over 11% Efficiency for Inverted Small-Molecule Organic Solar Cells." *Nat. Commun.* **2016,** *7*, 13740.

34. Wang, Y.; Zhang, Y.; Qiu, N.; Feng, H.; Gao, H.; Kan, B.; Ma, Y.; Li, C.; Wan, X.; Chen, Y. "A Halogenation Strategy for over 12% Efficiency Nonfullerene Organic Solar Cells." *Adv. Energy Mater.* **2018,** *8* (15), 1702870.

35. Stuart, A. C.; Tumbleston, J. R.; Zhou, H.; Li, W.; Liu, S.; Ade, H.; You, W. "Fluorine Substituents Reduce Charge Recombination and Drive Structure and Morphology Development in Polymer Solar Cells." *J. Am. Chem. Soc.* **2013,** *135* (5), 1806-1815.

36. Lu, L.; Yu, L. "Understanding Low Bandgap Polymer PTB7 and Optimizing Polymer Solar Cells Based on It." *Adv. Mater.* **2014,** *26* (26), 4413-4430.

37. Sun, H.; Tang, Y.; Koh, C. W.; Ling, S.; Wang, R.; Yang, K.; Yu, J.; Shi, Y.; Wang, Y.; Woo, H. Y.; Guo, X. "High-Performance All-Polymer Solar Cells Enabled by an n-Type Polymer Based on a Fluorinated Imide-Functionalized Arene." *Adv. Mater.* **2019,** *31* (15), 1807220.

38. Kawashima, K.; Fukuhara, T.; Suda, Y.; Suzuki, Y.; Koganezawa, T.; Yoshida, H.; Ohkita, H.; Osaka, I.; Takimiya, K. "Implication of Fluorine Atom on Electronic Properties, Ordering Structures, and Photovoltaic Performance in Naphthobisthiadiazole-Based Semiconducting Polymers." *J. Am. Chem. Soc.* **2016,** *138* (32), 10265-10275.

39. Yao, C.; Peng, C.; Yang, Y.; Li, L.; Bo, M.; Wang, J. "Elucidating the Key Role of Fluorine in Improving the Charge Mobility of Electron Acceptors for Non-Fullerene Organic Solar Cells by Multiscale Simulations." *J. Mater. Chem. C* **2018,** *6* (18), 4912-4918.

40. Meng, Y.; Wu, J.; Guo, X.; Su, W.; Zhu, L.; Fang, J.; Zhang, Z.-G.; Liu, F.; Zhang, M.; Russell, T. P.; Li, Y. "11.2% Efficiency All-Polymer Solar Cells with High Open-Circuit Voltage." *Sci. China Chem.* **2019,** *62* (7), 845-850.

41. Wu, J.; Meng, Y.; Guo, X.; Zhu, L.; Liu, F.; Zhang, M. "All-Polymer Solar Cells Based on a Novel Narrow-Bandgap Polymer Acceptor with Power Conversion Efficiency over 10%." *J. Mater. Chem. A* **2019,** *7* (27), 16190-16196.

42. Zhou, N.; Facchetti, A. "Naphthalenediimide (NDI) Polymers for All-Polymer Photovoltaics." *Mater. Today* **2018,** *21* (4), 377-390.

43. Yang, J.; Xiao, B.; Tang, A.; Li, J.; Wang, X.; Zhou, E. "Aromatic-Diimide-Based n-Type Conjugated Polymers for All-Polymer Solar Cell Applications." *Adv. Mater.* **2019,** *31*, 1804699.

44. Sun, H.; Wang, L.; Wang, Y.; Guo, X. "Imide-Functionalized Polymer Semiconductors." *Chem. Eur. J.* **2019,** *25* (1), 87-105.

45. Chen, D.; Yao, J.; Chen, L.; Yin, J.; Lv, R.; Huang, B.; Liu, S.; Zhang, Z.-G.; Yang, C.; Chen, Y.; Li, Y. "Dye-Incorporated Polynaphthalenediimide Acceptor for Additive-Free High-Performance All-Polymer Solar Cells." *Angew. Chem. Int. Ed.* **2018,** *57* (17), 4580-4584.

46. Zhang, N.; Xu, Y.; Zhou, X.; Zhang, W.; Zhou, K.; Yu, L.; Ma, W.; Xu, X. "Synergistic Effects of Copolymerization and Fluorination on Acceptor Polymers for Efficient and Stable All-Polymer Solar Cells." *J. Mater. Chem. C* **2019,** *7* (45), 14130-14140.

47. Liu, X.; Zou, Y.; Wang, H.-Q.; Wang, L.; Fang, J.; Yang, C. "High-Performance All-Polymer Solar Cells with a High Fill Factor and a Broad Tolerance to the Donor/Acceptor Ratio." *ACS Appl. Mater. Interfaces* **2018,** *10* (44), 38302-38309.

48. Zhang, M.; Guo, X.; Ma, W.; Ade, H.; Hou, J. "A Large-Bandgap Conjugated Polymer for Versatile Photovoltaic Applications with High Performance." *Adv. Mater.* **2015,** *27* (31), 4655-4660.

49. Earmme, T.; Hwang, Y.-J.; Murari, N. M.; Subramaniyan, S.; Jenekhe, S. A. "All-Polymer Solar Cells with 3.3% Efficiency Based on Naphthalene Diimide-Selenophene Copolymer Acceptor." *J. Am. Chem. Soc.* **2013,** *135* (40), 14960-14963.

50. Kulkarni, A. P.; Zhu, Y.; Babel, A.; Wu, P.-T.; Jenekhe, S. A. "New Ambipolar Organic Semiconductors. 2. Effects of Electron Acceptor Strength on Intramolecular Charge Transfer Photophysics, Highly Efficient Electroluminescence, and Field-Effect Charge Transport of Phenoxazine-Based Donorв€'Acceptor Materials." *Chem. Mater.* **2008,** *20* (13), 4212-4223.

51. Jenekhe, S. A.; Lu, L.; Alam, M. M. "New Conjugated Polymers with Donor-Acceptor Architectures: Synthesis and Photophysics of Carbazole-Quinoline and Phenothiazine-Quinoline Copolymers and Oligomers Exhibiting Large Intramolecular Charge Transfer." *Macromolecules* **2001,** *34* (21), 7315-7324.

52. Luna-Barcenas, G.; Meredith, J. C.; Sanchez, I. C.; Johnston, K. P.; Gromov, D. G.; de Pablo, J. J. "Relationship between Polymer Chain Conformation and Phase Boundaries in a Supercritical Fluid." *J. Chem. Phys.* **1997,** *107* (24), 10782-10792.

53. Williams, C.; Brochard, F.; Frisch, H. L. "Polymer Collapse." *Annual Review of Physical Chemistry* **1981,** *32* (1), 433-451.

54. Courtright, B. A. E.; Jenekhe, S. A. "Polyethylenimine Interfacial Layers in Inverted Organic Photovoltaic Devices: Effects of Ethoxylation and Molecular Weight on Efficiency and Temporal Stability." *ACS Appl. Mater. Interfaces* **2015,** *7* (47), 26167-26175.

55. Azzouzi, M.; Kirchartz, T.; Nelson, J. "Factors Controlling Open-Circuit Voltage Losses in Organic Solar Cells." *Trends in Chemistry* **2019,** *1* (1), 49-62.

56. Wang, Y.; Qian, D.; Cui, Y.; Zhang, H.; Hou, J.; Vandewal, K.; Kirchartz, T.; Gao, F. "Optical Gaps of Organic Solar Cells as a Reference for Comparing Voltage Losses." *Adv. Energy Mater.* **2018,** *8* (28), 1801352.

57. Ren, G.; Schlenker, C. W.; Ahmed, E.; Subramaniyan, S.; Olthof, S.; Kahn, A.; Ginger, D. S.; Jenekhe, S. A. "Photoinduced Hole Transfer Becomes Suppressed with Diminished Driving Force in Polymer-Fullerene Solar Cells While Electron Transfer Remains Active." *Adv. Funct. Mater.* **2013,** *23* (10), 1238-1249.

58. Duan, C.; Peng, Z.; Colberts, F. J. M.; Pang, S.; Ye, L.; Awartani, O. M.; Hendriks, K. H.; Ade, H.; Wienk, M. M.; Janssen, R. A. J. "Efficient Thick-Film Polymer Solar Cells with Enhanced Fill Factors via Increased Fullerene Loading." *ACS Appl. Mater. Interfaces* **2019,** *11* (11), 10794-10800.

59. Zhang, G.; Xia, R.; Chen, Z.; Xiao, J.; Zhao, X.; Liu, S.; Yip, H.-L.; Cao, Y. "Overcoming Space-Charge Effect for Efficient Thick-Film Non-Fullerene Organic Solar Cells." *Adv. Energy Mater.* **2018,** *8* (25), 1801609.

60. Jin, Y.; Chen, Z.; Xiao, M.; Peng, J.; Fan, B.; Ying, L.; Zhang, G.; Jiang, X.-F.; Yin, Q.; Liang, Z.; Huang, F.; Cao, Y. "Thick Film Polymer Solar Cells Based on Naphtho[1,2-c:5,6-c]bis[1,2,5]thiadiazole Conjugated Polymers with Efficiency over 11%." *Adv. Energy Mater.* **2017,** *7* (22), 1700944.

61. Fan, B.; Zhu, P.; Xin, J.; Li, N.; Ying, L.; Zhong, W.; Li, Z.; Ma, W.; Huang, F.; Cao, Y. "High-Performance Thick-Film All-Polymer Solar Cells Created Via Ternary Blending of a Novel Wide-Bandgap Electron-Donating Copolymer." *Adv. Energy Mater.* **2018,** *8* (14), 1703085.

62. Guo, B.; Li, W.; Guo, X.; Meng, X.; Ma, W.; Zhang, M.; Li, Y. "High Efficiency Nonfullerene Polymer Solar Cells with Thick Active Layer and Large Area." *Adv. Mater.* **2017,** *29* (36), 1702291.

63. Zhong, H.; Ye, L.; Chen, J.-Y.; Jo, S. B.; Chueh, C.-C.; Carpenter, J. H.; Ade, H.; Jen, A. K. Y. "A Regioregular Conjugated Polymer for High Performance Thick-Film Organic Solar Cells without Processing Additive." *J. Mater. Chem. A* **2017,** *5* (21), 10517-10525.

64. Huang, J.; Carpenter, J. H.; Li, C.-Z.; Yu, J.-S.; Ade, H.; Jen, A. K. Y. "Highly Efficient Organic Solar Cells with Improved Vertical Donor-Acceptor Compositional Gradient Via an Inverted Off-Center Spinning Method." *Adv. Mater.* **2016,** *28* (5), 967-974.

65. Wang, Z.; Hu, Y.; Xiao, T.; Zhu, Y.; Chen, X.; Bu, L.; Zhang, Y.; Wei, Z.; Xu, B. B.; Lu, G. "Correlations between Performance of Organic Solar Cells and Film-Depth-Dependent Optical and Electronic Variations." *Adv. Optical Mater.* **2019,** *7* (10), 1900152.

66. Proctor, C. M.; Kuik, M.; Nguyen, T.-Q. "Charge Carrier Recombination in Organic Solar Cells." *Prog. Polym. Sci.* **2013,** *38* (12), 1941-1960.

67. Cowan, S. R.; Banerji, N.; Leong, W. L.; Heeger, A. J. "Charge Formation, Recombination, and Sweep-Out Dynamics in Organic Solar Cells." *Adv. Funct. Mater.* **2012,** *22* (6), 1116-1128.

68. A. Street, R.; Cowan, S.; J. Heeger, A. "Experimental Test for Geminate Recombination Applied to Organic Solar Cells." *Phys. Rev. B* **2010,** *82*, 121301(R).

69. Jenekhe, S. A.; Osaheni, J. A. "Excimers and Exciplexes of Conjugated Polymers." *Science* **1994,** *265* (5173), 765-768.

70. Xie, B.; Zhang, K.; Hu, Z.; Fang, H.; Lin, B.; Yin, Q.; He, B.; Dong, S.; Ying, L.; Ma, W.; Huang, F.; Yan, H.; Cao, Y. "Polymer Pre-Aggregation Enables Optimal Morphology and High Performance in All-Polymer Solar Cells." *Solar RRL* **2019,** *n/a* (n/a), 1900385.

71. Kim, M.; Kim, J.-H.; Choi, H. H.; Park, J. H.; Jo, S. B.; Sim, M.; Kim, J. S.; Jinnai, H.; Park, Y. D.; Cho, K. "Electrical Performance of Organic Solar Cells with Additive-Assisted Vertical Phase Separation in the Photoactive Layer." *Adv. Energy Mater.* **2014,** *4* (2), 1300612.

72. Liu, S.; Chen, D.; Zhou, W.; Yu, Z.; Chen, L.; Liu, F.; Chen, Y. "Vertical Distribution to Optimize Active Layer Morphology for Efficient All-Polymer Solar Cells by J71 as a Compatibilizer." *Macromolecules* **2019,** *52* (11), 4359-4369.

73. Huang, L.; Wang, G.; Zhou, W.; Fu, B.; Cheng, X.; Zhang, L.; Yuan, Z.; Xiong, S.; Zhang, L.; Xie, Y.; Zhang, A.; Zhang, Y.; Ma, W.; Li, W.; Zhou, Y.; Reichmanis, E.; Chen, Y. "Vertical Stratification Engineering for Organic Bulk-Heterojunction Devices." *ACS Nano* **2018,** *12* (5), 4440-4452.

74. Jasieniak, J. J.; Treat, N. D.; McNeill, C. R.; de Villers, B. J. T.; Della Gaspera, E.; Chabinyc, M. L. "Interfacial Characteristics of Efficient Bulk Heterojunction Solar Cells Fabricated on MoO_x Anode Interlayers." *Adv. Mater.* **2016,** *28* (20), 3944-3951.

75. Hwang, Y.-J.; Murari, N. M.; Jenekhe, S. A. "New N-Type Polymer Semiconductors Based on Naphthalene Diimide and Selenophene Derivatives for Organic Field-Effect Transistors." *Polym. Chem.* **2013,** *4* (11), 3187-3195.

76. Westenhoff, S.; Howard, I. A.; Friend, R. H. "Probing the Morphology and Energy Landscape of Blends of Conjugated Polymers with Sub-10 nm Resolution." *Phys. Rev. Lett.* **2008,** *101* (1), 016102.

77. Najafov, H.; Lee, B.; Zhou, Q.; Feldman, L. C.; Podzorov, V. "Observation of Long-Range Exciton Diffusion in Highly Ordered Organic Semiconductors." *Nat. Mater.* **2010,** *9* (11), 938-943.

Table of content graphics: